Global and Planetary Change 171 (2018) 185–206

Contents lists available at ScienceDirect

Global and Planetary Change

journal homepage: www.elsevier.com/locate/gloplacha

Structural controls on sedimentation during asymmetric extension: The case of Sorbas Basin (SE Spain)

Nevena Andrić[a,b,*], Liviu Matenco[a], Frits Hilgen[a], Hans de Bresser[a]

[a] Utrecht University, Faculty of Geosciences, Department of Earth Sciences, Utrecht, The Netherlands
[b] University of Belgrade, Faculty of Mining and Geology, Belgrade, Serbia

A B S T R A C T

Understanding the link between sedimentation and fault kinematics is important for reconstructing the evolution of sedimentary basins. The relationship between the mechanics of creating accommodation space and the sediment supply in asymmetric extensional basins is critical for quantifying their syn- and post-rift evolution, but is not yet well understood. One exceptional place to analyze such mechanics of normal faulting and its relationship with the evolution of depositional environments is the Sorbas Basin in the Betic Cordillera of SE Spain. We have analyzed the interplay between extension and deposition by means of a detailed sedimentological and field kinematic study. The results indicate a novel and coupled evolution, characterized by low-order tectonically induced sedimentary successions driven by the change of deformation style and high-order tectonically induced sedimentary successions driven by individual stages of fault activity. Fault mechanics and hanging-wall tilting control the formation of depositional slopes, while footwall exhumation induces enhanced sourcing of coarse sediments that may be stored in proximal areas or recycled in the basin during episodes of fault activity. Following initiation of extension, the subsequent syn-kinematic deposition was characterized by a wide spectrum of subaqueous gravity flows, whose types and transformation mechanisms were controlled by the style of normal faulting, sediment supply and basin physiography. Furthermore, the study quantifies the controls of rheological stratified sediments on normal faulting mechanics and their implications for the spatial and temporal basin evolution.

1. Introduction

The architecture of sedimentary basins is controlled by the balance between the rate of creating accommodation space and the rate of sediment supply (e.g., Schlische, 1991; Schlager, 1993; Gawthorpe et al., 1994). The kinematics and offset of normal faults dominantly control the sediment production and dispersal patterns in extensional basins by creating the accommodation space, influencing the basin physiography, drainage network and sediment transport pathways (e.g., Colella, 1988; Gupta et al., 1999; Whittaker et al., 2007; Ge et al., 2017). The variability and evolution of normal fault offsets or migration of deformation across fault arrays creates tectonic-induced sedimentary successions that have a wide range of time scales, from millions to several thousand years (e.g., Gawthorpe and Leeder, 2000; Petersen et al., 2010). These sedimentary successions record the system response to the onset of fault activity and/or perturbation of its slip rates (e.g., Whittaker et al., 2007; Armitage et al., 2011; Stojadinović et al., 2017).

The sediment distribution is also controlled by other external and internal forcing factors, such as the variability of climate (precipitation and evapo-transpiration), sea-level variations and autogenic processes, such as turbiditic/deltaic lobes switching or the development of temporary sediment storages (e.g., Castelltort and Van Den Driessche, 2003; Folkestad and Satur, 2008; Jackson et al., 2010; García-García et al., 2011). These forcing factors leave typical signatures in the sedimentary record, such as coarsening- and/or thickening-upward and fining- and/or thinning-upward patterns (e.g., Prélat et al., 2009; Martins-Neto and Catuneanu, 2010). Disentangling the effects of tectonics from these other forcing factors to derive the mechanics of extensional basins is often challenging and usually relies on the observation of different orders of cyclicity in depositional packages and their relationship with basin-wide deformation features (e.g., García-García et al., 2006; Armitage et al., 2011).

Much less is known on the relationship between the mechanics of normal faulting and the outcrop-scale climatic and autogenic response of system, when compared with the conceptual availability of regional tectonic system tracts or other more general syn- and post-rift types of deposition (e.g., Prosser, 1993; Nottvedt et al., 1995; Martins-Neto and Catuneanu, 2010; Balázs et al., 2016; Andrić et al., 2017). The initiation

* Corresponding author at: Utrecht University, Faculty of Geosciences, Department of Earth Sciences, PO Box 80021, 3508TA Utrecht, The Netherlands.
E-mail address: n.andric@uu.nl (N. Andrić).

https://doi.org/10.1016/j.gloplacha.2018.01.019
Received 5 July 2017; Received in revised form 18 November 2017; Accepted 14 January 2018
Available online 31 January 2018
0921-8181/

of extension is often associated with the deposition of coarse-grained alluvial fans and/or fan deltas sourced from uplifting footwalls and deposited along extensional margins at the base of fault scarps (e.g., Colella, 1988; Postma and Drinia, 1993; Leppard and Gawthorpe, 2006). Owing to the proximity to the active normal fault, these relatively small-scale depositional systems respond rapidly to slip events, which are observed in the alternation of vertical coarsening- and/or fining-upward trends (e.g., Rohais et al., 2008). The initiation of normal faulting creates a gradually increasing depositional slope that delivers gravity flow sedimentation to the deep-water environment (e.g., Nemec, 1990; Fugelli and Olsen, 2007; Strachan et al., 2013). During rapid sedimentation associated with normal faulting, terrigenous or shallow marine material may be delivered as out-sized coarser-grained events into an otherwise contrasting deep-water facies, for instance coarse deposition in distal prodelta mudstones (Young et al., 2000) or distal deep marine lobes (Kane et al., 2017). Furthermore, large-scale slide and debris flow deposits are shed by slope collapse into the deep-water facies (e.g., Kleverlaan, 1987). However, a direct observation of the relationship between these types of flows and their changes controlled by the activity of normal faults and other forcing factors (eustasy, climate, runoff precipitation, autocyclic processes) is very rare in outcrop studies (Henstra et al., 2016), but is important to understand the mechanics of deformation.

One excellent example of a basin preserving extensive exposures of sedimentary facies deposited during the initiation of extension is the Sorbas Basin, part of the extensional system overlying the internal parts of Betic Cordillera in the SE Spain (Fig. 1; e.g., Dewey et al., 1989; Rosenbaum et al., 2002; Vissers, 2002). Exposures of normal faults and associated syn-kinematic sedimentary facies deposited during the Upper Serravallian-Tortonian initiation of extension are available in the SE part of the Sorbas Basin (e.g., Haughton, 1994; Do Couto et al., 2014 and references therein). In this part of the basin, we have studied the link between normal faulting and continental to deep-water deposition by means of a high resolution kinematic and sedimentological study. The aim is to quantify the influence of the change in slope and bathymetry induced by normal faulting, and the associated sedimentary flow dynamics and lobe stacking patterns, while the climatic and autogenic effects are discriminated through comparison with the extensive work available in previous studies of the Sorbas and neighbouring basins (e.g., Haughton, 2001; Puga-Bernabéu et al., 2007a, 2007b; Sanchez-Almazo et al., 2007; Postma et al., 2014 and references therein). The results are integrated in a dynamic model of sedimentation during initiation of extension and are discussed in the overall context of the Betic Cordillera evolution.

2. Geological setting

The Betic-Rif orogenic system (Fig. 1a, b) formed in response to the subduction and closure of the Tethyan ocean during the convergence between the Iberia and Africa continental units (e.g., Balanyá and García-Dueñas, 1987; Lonergan and White, 1997; Martínez-Martínez and Azañón, 1997; Duggen et al., 2004; Vissers, 2002). The late Mesozoic to Cenozoic shortening resulted in the creation of a nappe stack affecting Palaeozoic-Mesozoic sediments derived from the southern Iberian margin in the External Betics or derived from the southern Iberian and Alboran margins in the Internal Betics (the Nevado-Filabride, Alpujarride and Malaguide units, García-Hernández et al., 1980; Banks and Warburton, 1991; Platt et al., 2003; Balanyá et al., 1997; Torres-Roldan, 1979). The Oligocene–early Miocene shortening in the External Betics was largely coeval with extensional deformation in the

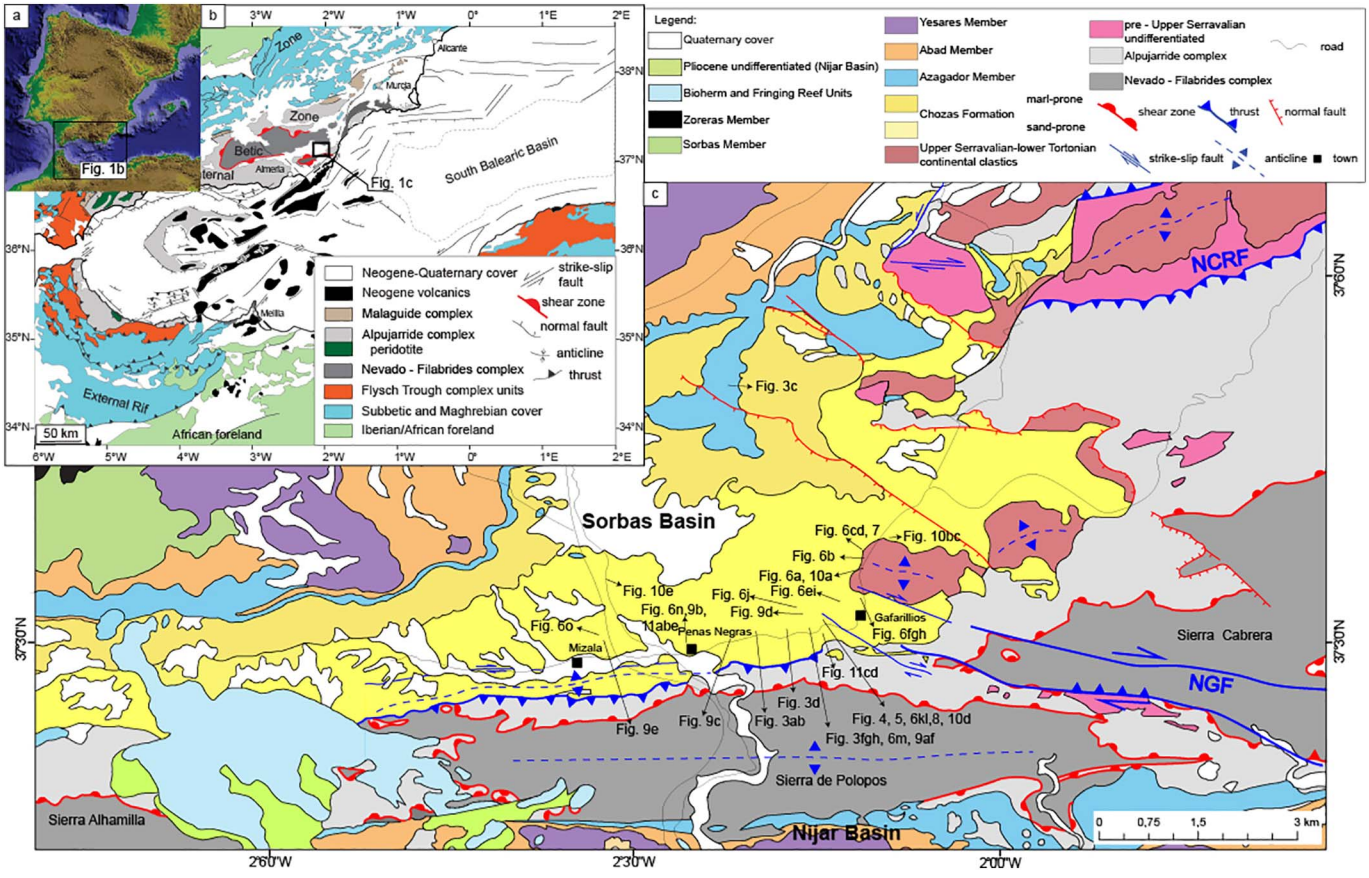

Fig. 1. a) Simplified map of the Iberian Peninsula with the location of the Betic and Rif system b; b) tectonic map of the Betic-Rif orogenic system (modified after Comas et al., 1999). The thick rectangle shows the study area of c; c) geological map of the SE part of Sorbas basin (modified after Do Couto et al., 2014). NGF-North Gafarillos fault, NCRF-North Cabrera reverse fault, and SGF-South Gafarillos fault.

Internal Betics. This extension partly reactivated former thrusts as detachments and induced a rapid exhumation of metamorphic cores (e.g., Martínez-Martínez and Azañón, 1997; Platt and Vissers, 1989; Platt et al., 2005; García-Dueñas et al., 1992; Augier et al., 2005a, 2005b). The exhumation was kinematically associated with the formation and evolution of several extensional basins that presently separate the metamorphic sierras of the SE Spain (Fig. 1b, García-Dueñas et al., 1992; Lonergan and Platt, 1995; Crespo-Blanc et al., 1994; Augier et al., 2005a, 2005b; Meijninger, 2006; Pedrera et al., 2012; Giaconia et al., 2014). The overall extension is generally thought to be driven by removal of lithospheric mantle beneath the Internal Betics or by roll-back associated with detachment of the Gibraltar slab (e.g., Faccenna et al., 2004; Spakman and Wortel, 2004; Jolivet et al., 2008; Gutscher, 2012; Vissers, 2002). The initial early Miocene (~22 to 18 Ma) N-S to NNE-SSW oriented extension was associated with the exhumation of the neighbouring Alpujarride and Nevado-Fillabrides nappe complex (e.g. Monié et al., 1991; Crespo-Blanc et al., 1994; Platt et al., 2005) and was followed by an E-W oriented middle–late Miocene (~15 to 9 Ma) extension driving the main subsidence observed in the basins (e.g., De Jong, 1991; Jabaloy et al., 1992; Johnson et al., 1997; Augier et al., 2005a, 2005b; Platt et al., 2005; Vázquez et al., 2011).

The Sorbas Basin, situated in the Internal Betics (Fig. 1b, c) was analyzed in numerous studies, owing to the extended and almost complete exposure of its middle Miocene–Pliocene fill (e.g., Do Couto et al., 2014 and references therein). The Sorbas Basin is flanked by metamorphic rocks of the Sierra Alhamillia, Sierra de Polopos and Sierra Cabrera to the south and the Sierra de los Filabres to the north (Fig. 1). These sierras are generally slightly asymmetric domes with structurally steep northern flanks and gentle dipping southern ones (e.g., Platt and Vissers, 1989). The basement of these sierras (Fig. 1) is made up by a nappe stack composed of low-temperature and locally high-pressure Alpujarride and high-temperature and locally high-pressure, Nevado-Filabride meta-sediments and magmatics (Johnson et al., 1997; Martínez-Martínez and Azañón, 1997; Booth-Rea et al., 2002, 2005 Vázquez et al., 2011. This nappe stack was partly reactivated during the onset and evolution of a large scale ductile and brittle Miocene extensional structure (the Betic Movement Zone, e.g., Vissers, 2002; Platt et al., 2013).

The oldest Miocene sediments are poorly preserved Burdigalian (-Langhian?) marly limestones, sandstones, conglomerates and marls observed as isolated patches overlying the basement of Sierra Cabrerra (pre-late Serravalian in Fig. 1c, Ott d'Estevou et al., 1990; De Galdeano and Vera, 1992). Their deposition is thought to have been controlled by an earlier extensional episode associated with the exhumation of the basement nappe stack (22–18 Ma, e.g., Crespo-Blanc et al., 1994). The subsequent deposition in the Sorbas Basin was driven by extension, followed by inversion and influenced by the large sea-level changes during the Messinian Salinity Crisis (Fig. 1c, Martín and Braga, 1994; Stapel et al., 1996; Hodgson and Haughton, 2004).

The late exhumation stages of the Nevado-Filabrides during the late Serravallian to early Tortonian was coeval with the main onset of sedimentation in the Sorbas Basin (~12–11 Ma, Johnson et al., 1997; Vázquez et al., 2011; Augier et al., 2013). The extension has created an asymmetric geometry. Recent studies have shown that the basin evolution was controlled by the activity of listric normal faults that converged at depth into in a low-angle detachment observed in the exposed metamorphic rocks of the Nevado-Filabrides unit and are presently buried at < 1 km beneath the Miocene sediments in the SE part of the basin (Fig. 1, Li et al., 2012; Giaconia et al., 2014; Do Couto et al., 2014). Furthermore, these faults are segmented by strike-slip faults, which acted as lateral ramps for the subsequent inversional deformation (Giaconia et al., 2014). The main extensional evolution started in the Sorbas Basin at ~12–11 Ma (Fig. 2) during the extensional exhumation of the Nevado-Filabrides unit (e.g., Johnson, 1993; Johnson et al., 1997; Augier et al., 2013). The subsidence was driven by successive episodes of NW-SE and NE-SW presently oriented extension directions, which controlled the sedimentation during the late Serravallian-Tortonian (e.g., Do Couto et al., 2014 and references therein). The associated sedimentation is made up by fluvial conglomerates, sandstones and siltstones that laterally grade into deltaic conglomerates, sandstones and marls that reach thicknesses of ~100 m (e.g., Ott d'Estevou et al., 1990). The gradually increasing Tortonian normal faulting accelerated the basin subsidence and created an open marine environment (e.g., Dabrio, 1990; Poisson et al., 1999), where a deltaic system was shedding conglomerates and sandstones that were transported further into the basin by turbiditic submarine fan systems interbedded within pelagic marls (e.g. Haughton, 2001). These sediments are ~2 km thick and are generally grouped into the generic Chozas Formation (e.g., Völk, 1966; Ott d'Estevou et al., 1990; Barragán, 1997). During the late Tortonian, the basin was predominately supplied by north to south directed flows (i.e. sediments derived from Sierra de los Filabres). Further into the basin, the flows were deflected along the northern margin of Sierra Alhamillia, which resulted in a dominant west to east flow direction (e.g., Weijermars et al., 1985; Haughton, 2001). The Chozas Formation shows progressive younging westwards, while the eastern part of the basin was deformed and inverted during the late Tortonian (e.g., Haughton, 2000; Haughton, 2001). Therefore, the upper part of the turbiditic sequence is considered to have been deposited during the subsequent inversion and strike-slip faulting observed with larger effects near the southern basin margin, which has influenced the depositional character of this sequence (e.g., Kleverlaan, 1989; Poisson et al., 1999; Haughton, 2001).

The upper Tortonian turbidites (Chozas Formation) are overlain by shallow-water temperate ramp carbonates, generally grouped into an uppermost Tortonian to lowermost Messinian Azagador Member that belongs to the Turre Formation (Fig. 2, e.g., Völk and Rondeel, 1964; Ruegg, 1964; Martín et al., 1999; Braga et al., 2006; Puga-Bernabéu et al., 2007a, 2007b). The contact between the Chozas Formation and the Azagador Member is thought to be an unconformity, which recorded the latest Tortonian–earliest Messinian phase of basin inversion (e.g., Poisson et al., 1999). The Azagador carbonates prograded basinwards, have a gradual transition to and are overlain by more distal marls (the Lower Abad Member, e.g., Ruegg, 1964; Riding et al., 1991; Martín and Braga, 1994). At the beginning of Messinian times both the southern and the northern basin margins were overstepped by reef deposits (Bioherm Unit and Fringing Reef Unit, respectively, part of the Turre Formation), which were locally deposited unconformably on top of the Azagador Member (e.g., Ruegg, 1964; Martín and Braga, 1994; Riding et al., 1991). Basin-wards, these reef units grade laterally into silty marls and marls intercalated with diatomites (the Upper Abad Member of the Turre Formation, e.g., Völk and Rondeel, 1964; Ruegg, 1964, Krijgsman et al., 2001). During the Messinian Salinity Crisis, the Sorbas Basin became progressively more isolated. This isolation started at 5.971 Ma and led to deposition of 120 m thick selenite gypsum, interbedded within clay and marly laminites (the Yesares Formation, Dronkert, 1976; Van de Poel, 1991; Manzi et al., 2013). These evaporites are overlain by lagoonal coarse carbonates that laterally grade into Gilbert type of delta deposits (the Sorbas Member of the Canos Formation, e.g., Völk and Rondeel, 1964; Roep et al., 1998). The whole succession was covered by red continental conglomerates that reach ~60 m in thickness (the Zorreras Member of the Canos Formation, Völk and Rondeel, 1964; Montenat et al., 1980; Martín-Suárez et al., 2000).

The southern boundary of the basin (the northern limit of Sierra de Polopos and Sierra Alhamillia, Fig. 1) is part of a transpressive fault system with top NW sense of shear that formed during an episode of late Tortonian-Messinian basin inversion, which possibly reactivated earlier extensional normal faults (e.g., Ott d'Estevou et al., 1990; Haughton, 2001; Giaconia et al., 2012a, 2012b, 2013; Jonk and Biermann, 2002; Booth-Rea et al., 2002, 2005). In the SE, this transpressive deformation is made up by the Gafarillos Fault, which has a northern and a southern branch (Fig. 1b, e.g., Giaconia et al., 2012a, 2012b, 2013). The inversion is thought to have migrated westwards with time (e.g. Jonk and

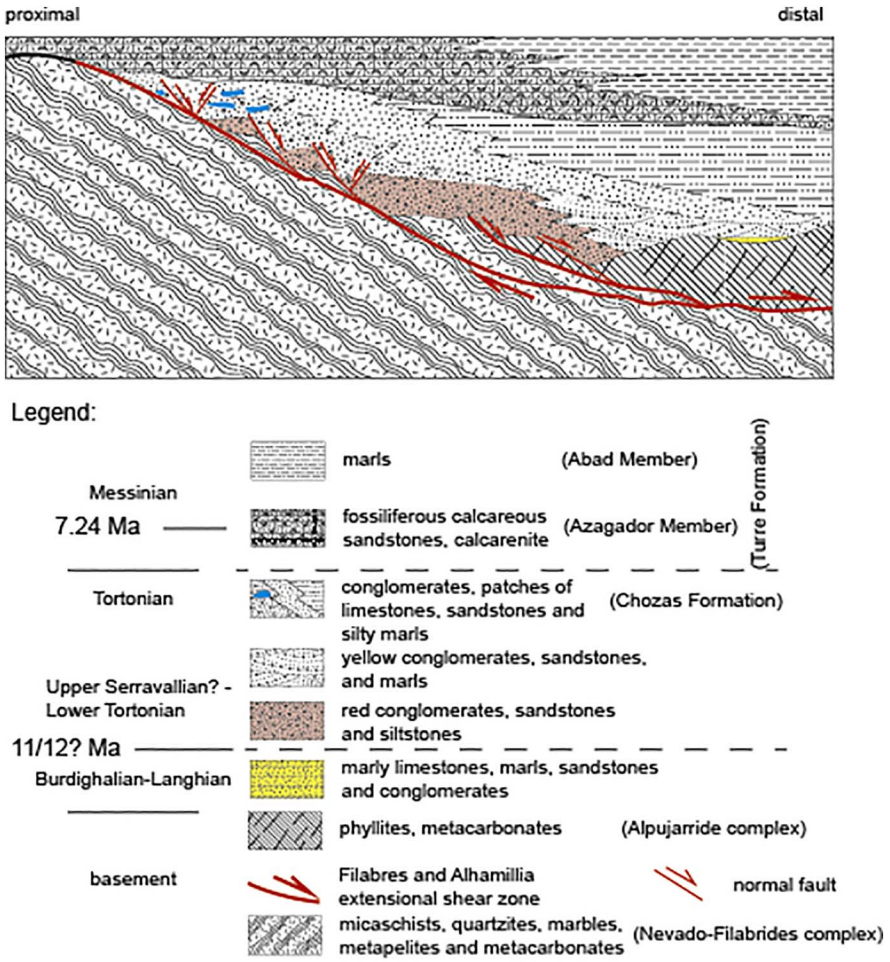

Fig. 2. General lithostratigraphic scheme of the Sorbas Basin, modified from Puga-Bernabéu et al. (2007a, 2007b), Ott d'Estevou et al. (1990) and the results of the present study.

Biermann, 2002; Giaconia et al., 2012a, 2012b) and was associated with the deposition of upper Tortonian sediments (e.g., Weijermars et al., 1985; Kleverlaan, 1989). The overall inversion is thought to have started at ~8 Ma and was driven by N-S contraction and transcurrent deformation post-dating the back-arc extension, as observed elsewhere in the Alboran Domain (e.g., Comas et al., 1999; Jolivet et al., 2008).

3. Methodology

Understanding the link between the formation of normal faults at outcrop scale and the response in sedimentation requires a dual structural and sedimentological approach in an area with very good and continuous exposures during the onset of extension. Previous studies have shown that such continuous exposures during the onset of extension are available in the SE part of the Sorbas Basin, in the area immediately adjacent to the basement and Mesozoic cover of Sierra Cabrerra and Sierra de los Polopos (Fig. 1, e.g., Do Couto et al., 2014 and references therein). These studies have also shown that the extensional basin fill of the Sorbas Basin has been partly exhumed in this area by the subsequent inversion in such a fashion that the original ductile to brittle detachment and the normal faults bounding the basin have been significantly eroded (Fig. 2). This has created an opportunity to study both the earlier formed normal faults during the onset of continental sedimentation and the later ones formed during the transition to marine turbiditic deposition. Therefore, we have focussed our high-resolution study in this SE part of the basin and upwards in the stratigraphy in sediments as young as the Azagador Member (Figs. 1b and 2). The continuous outcrops show that the extensional deformation and associated sedimentological changes are particularly intense in the vicinity of the southern inversional fault in the area of the Gafarillos and Penas Negras villages (Fig. 1c), while the deformation decreases upwards in the stratigraphy. Therefore, most of our observations are focussed in the area of these villages, being less illustrative elsewhere for the link between normal faulting and sedimentation.

Structural observations were performed by standard kinematic mapping of deformation structures, such as faults and folds. The sense of shear along faults was derived from kinematic indicators such as Riedel shears, drag folds and slickenslides. Whenever required, faults and folds have been restored to their original position prior to inversion by using bedding measurements and calculating depositional slopes, based on for instance progradation or deltaic topsets–foresets-bottomsets geometries visible in outcrops. Superposition of deformation was determined at first by cross-cutting relationships of faults, commonly used in other structural studies of the Sorbas Basin (Do Couto et al., 2014; Giaconia et al., 2014). However, different from these studies, the relative age of deformation was derived primarily from a stratigraphic correlation of the observed syn-kinematic wedges in the hanging-wall and associated erosion in the footwall of faults. Faults were grouped in systems that were observed to merge in splaying structures, which were furthermore ordered in deformation events based on the stratigraphy of the syn-kinematic wedges (Figs. 3 and 4). Given the common observation of contrasting rheologies cross-cut by faults, such as strong rheologies in consolidated conglomerates or coarse sandstones and weak rheologies in poorly consolidated silts or shales, special attention was devoted to mapping the geometry and kinematics of fault segments at their transition.

Structural observations were combined with detailed sedimentological observations in the same transitional area from continental to

marine deposition in the SE part of the Sorbas Basin. The continuous outcrops were logged along multiple sections by following vertical and horizontal facies variations, aided by the interpretation at the scale of individual beds of large panoramic photos. This has allowed the definition of 18 facies units based on lithology, structure, texture, contacts with underlying and overlying units, fossil content and color (Table 1, e.g., Miall, 1996; Folkestad and Satur, 2008). These facies units were subsequently grouped by the definition of 8 facies associations in the observed alluvial fan and shallow marine, deltaic and deeper marine depositional system by following a standard sedimentological procedure (Table 1, e.g., Leppard and Gawthorpe, 2006; Strachan et al., 2013). Given the frequent observation of depositional events characterized by contrasting lithologies, a special attention was dedicated to the mapping and understanding of such 'event beds', which furthermore aided in the definition of flow types, which are related or not with episodes of normal faulting.

Following the understanding of normal faults kinematics and associated sedimentation, the asymmetric deposition of syn-kinematic wedges in the hanging-wall of normal faults demonstrates directly their tectonic genesis. This has allowed the definition of a high-order sedimentological cycles (or successions) controlled by the evolution of observed normal faults in the studied part of the Sorbas Basin. Grouping these cycles and correlating them to data from available studies on autogenic sedimentation and climatic effects has allowed the definition of a low-order tectonic-driven sedimentary cycles (or successions). These successions were formed during different evolutionary stages of the asymmetric extensional Sorbas Basin, which is furthermore discussed in phenomenological context.

4. Field observations of faults and their interpretation

4.1. Fault orientations and general geometries

A large number of normal faults were mapped in the basin, in

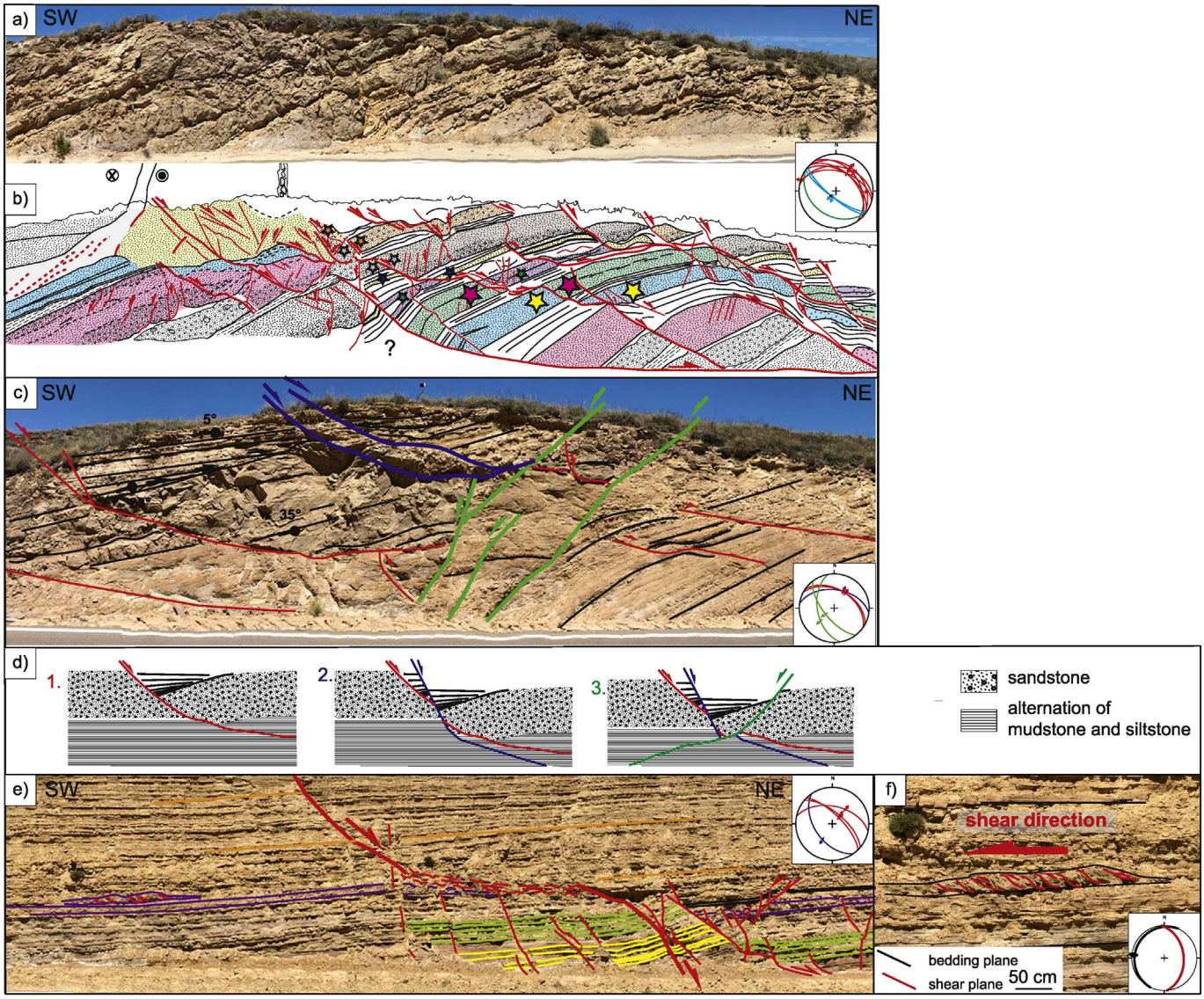

Fig. 3. Extensional geometries and kinematics of normal faulting in the turbiditic succession of the Chozas Formation in the SE part of Sorbas Basin. Locations in Fig. 1c. a) Panoramic photo and b) interpretation of normal faulting associated with deformation along an extensional ramp-flat system and associated syn-kinematic deposition in a submarine fan environment. Green line, blue and red lines on the stereonet represent bedding plane, antithetic and synthetic faults; c) intersection of successive stages of high- and low-angle normal faults. Note the refraction at the transition between thick sandstones and mudstones/siltstones layers; d) Evolutionary sketch of the three successive deformation events depicted in c. The oldest faults are associated with syn-kinematic sedimentation; e) extensional ramp-flat geometry formed in sediments of facies association C5, where the flat segment truncates mud-rich sandstones, and; f) raft of thrusts that formed originally in the lower part of a toe slope décollement. (For interpretation of the references to color in this figure legend, the reader is referred to the web version of this article.)

particular in the SE-part where the upper Serravallian-Tortonian fluvial, deltaic and offshore marine successions crop out (Figs. 3–5). Many of these faults show variable offsets, reaching few tens of metres in the studied outcrops (e.g., Figs. 3b, 4b, 5f). In addition, bed thicknesses regularly vary between hanging wall and footwall in response to the deposition of wedge shaped sediments that contain often chaotic packages of autochthonous material and intra-basinal clasts. These wedges were deposited during the formation of normal faults, as demonstrated by their deposition in the immediate hanging-wall and the gradual change in fault offset in their upper part (Figs. 4b and 10). When faults are not reactivated, these offsets decrease to zero in the upper part of these clear syn-kinematic wedges associated with the normal faulting. These normal faults are often organized in conjugate sets and are locally connected along their strike by less frequent E-W oriented strike-slip faults.

The oldest upper Serravalian–Tortonian sequence exposed near the Gafarillos village (Fig. 1c) is affected by a particularly dense array of normal faults. The frequency of these faults rapidly decreases upwards in the stratigraphy. The faults affect the fluvial, deltaic and the transition to submarine fan deposits (Figs. 3 and 4), and have two main directions of extension, NW-SE and NE-SW. The NW-SE direction of extension is predominant in the older alluvial to deltaic sequence located in the SE part of the basin. These faults have centimetres to metres offsets, with a few examples reaching > 10 m (e.g. Fig. 4b). The NE-SW direction of extension is dominant upwards in the stratigraphy. Both sets of normal faults often show high-angle or ramp geometries in conglomerates and thick sandstones, and listric or layer parallel fault segments in finer geometries (Figs. 4 and 5). Large offset faults are associated with antithetic tilting of hanging-walls, folding and draping geometries in finer sediments, and coarse lithologies deposited near fault planes. In more uniform lithologies, similar antithetic tilting is observed along successive fault arrays ("domino" normal faulting, Fig. 10c, e).

Upwards in the stratigraphy of the Chozas Formation (such as exposed along the road linking Penas Negras and Gafarillos, Fig. 1c) normal faults with variable offsets (cm to > 20 m) have a dominant top to the NE sense of tectonic transport and have more complex geometries when compared with the lower alluvial part of succession (Figs. 4 and 5). The faults show ubiquitous ramp-flat (Fig. 3a, b, e), complex listric (Fig. 3c) or staircase (Fig. 4) geometries. Simple planar or listric geometries are less frequent (Fig. 4c). Low angle normal faulting is observed in matrix-supported, and/or semi-lithified sandstones and

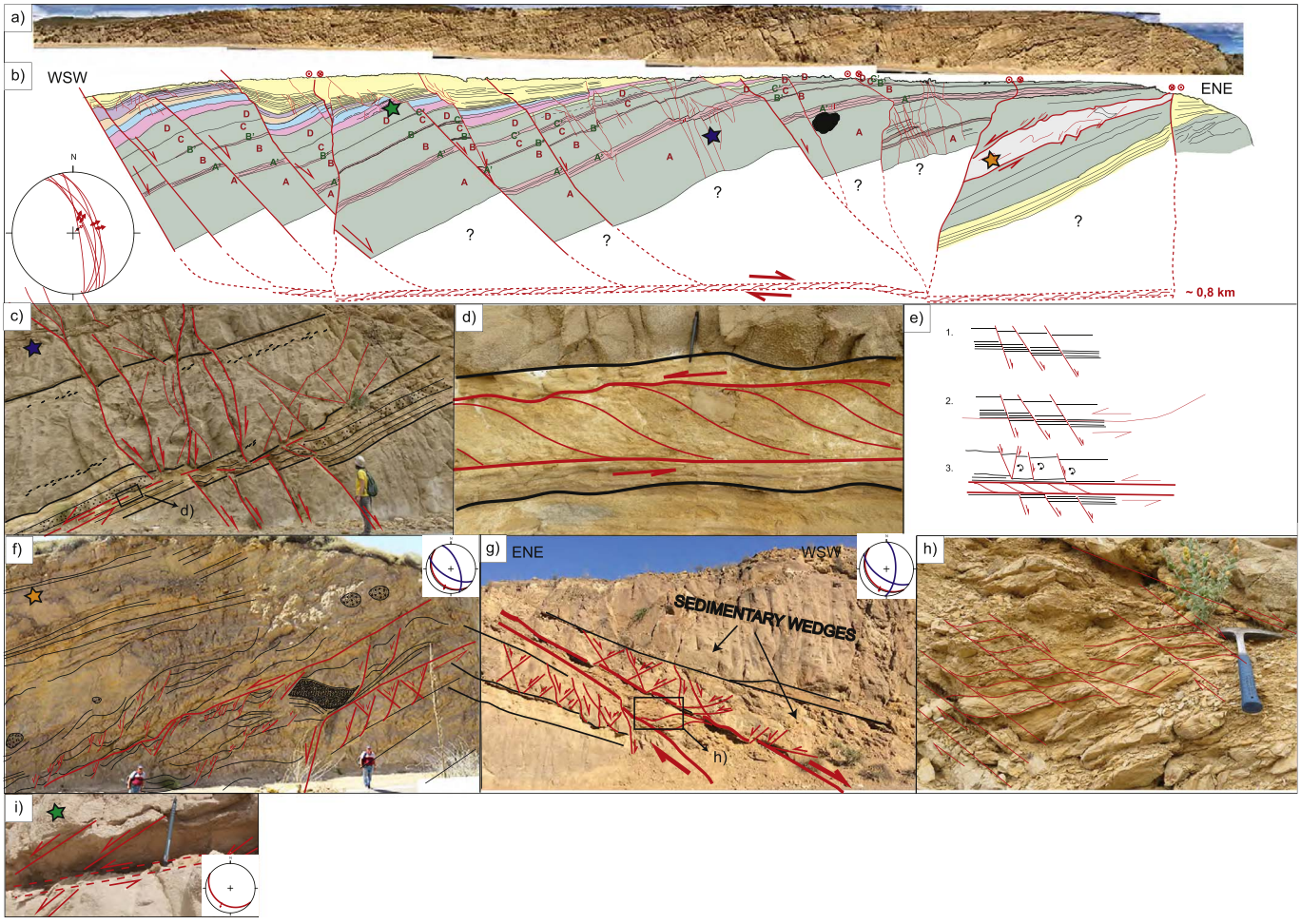

Fig. 4. Extensional geometries and kinematics of normal faulting in the shallow water deltaic to submarine fan transition cropping out in the SE part of Sorbas Basin. Locations in Fig. 1c. a) Panoramic photo and b) interpretation of a listric normal fault system dipping ENE-wards truncated by subsequent strike-slip structures formed during basin inversion. Note the antithetic tilting of hanging-walls that created the main depositional slope of the basin; c) intersection between two normal fault sets cross-cutting a thick event bed (location is the blue star in b); d) inset of c illustrating layer parallel shearing in the fine-grained sediments; e) possible solution for the temporal evolution of fault sets depicted in b: the flat segment forms as layer-parallel shear zone that formed subsequently and cross-cuts the earlier domino-style normal faults; f) large-scale extensional shear zone formed along a SW dipping normal fault (location is the orange star in b). Riedel shears are domains where less deformed, but rheologically strong layers (sandstones and conglomerates) form sigmoidal clasts that may reach up to 2 m; g) variability of the same shear zone as in f towards the south. Earlier formed conjugate normal faults are truncated by the shear zone; h) inset of g illustrating CS structural fabrics developed within shear zone, and; i) layer parallel shearing developed within rheologically weak layers (location is the green star in b). (For interpretation of the references to color in this figure legend, the reader is referred to the web version of this article.)

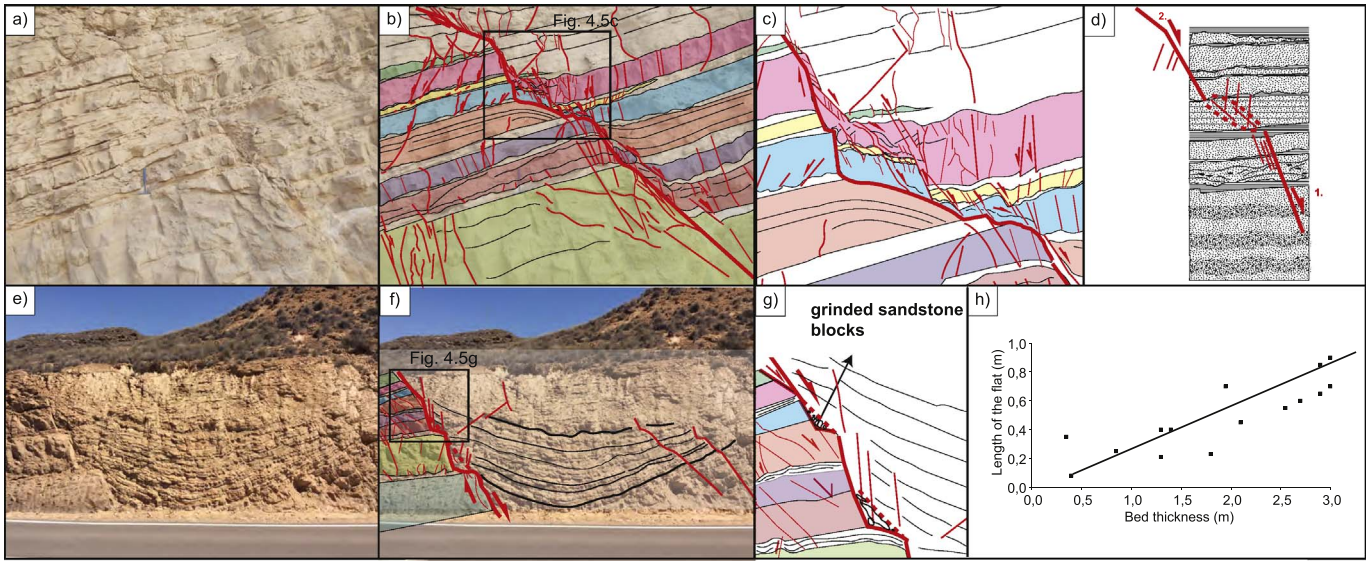

Fig. 5. Illustration of normal faults with staircase geometry. Locations in Fig. 1c. a) Photo and b) interpretation sketch of fault with a staircase geometry. The transition between segments is observed along layer parallel surfaces (flats) that truncate a sandstone/silty lithology; c) inset of b illustrating an extensional horse formed along a step in the staircase geometry. Well-cemented sandstone blocks are rotated, while the weaker silty sandstones and mudstones are sheared, forming an overall sigma-like clast geometry; d) sketch illustrating the mechanisms of connecting two highly-inclined segments of the staircase geometry by deforming a restraining vertical overlap zone (red dashed line); e) photo and f) interpretation of a large offset normal fault with a staircase geometry; g) inset of f, illustrating shortcutting the steps of a staircase geometry forming grinded sandstone and mudstone in the damage area, and; h) the observed correlation between the length of the flat segment and the thickness of underling rheological strong layers observed along the staircase fault trace geometry. (For interpretation of the references to color in this figure legend, the reader is referred to the web version of this article.)

conglomerates (Figs. 3a, b, e and 4). Normal faulting initiated with Riedel shears and created fault gouges and semi-ductile shear zones in finer silt or shale lithologies (Fig. 4d–h). This faulting is associated with numerous connecting joints and Riedel shears.

4.2. Fault characteristics in relation to lithology

A characteristic ramp-flat geometry of large NE-dipping faults is often observed within heterogeneous sediments deposited in deltaic and deep-water settings and such faults are often associated with syn-kinematic clastic wedges (Fig. 3a, b, c). Ramps are observed in sandstones and conglomerates, often at right angles to bedding (Fig. 3a, b). Flats are observed in finer silt or shale lithologies, where shearing is observed by the formation of brittle shear-bands and sheared clasts geometries in a fault gouge that is usually foliated. Deformation is associated with joints, antithetic Riedel shears, roll-over anticlines and small (half-) grabens located in hanging walls (Figs. 3a, b and 4a, b).

Foliated fault gouges are made up of silt and clay material, may reach 5 m thickness and show clear shear-sense indicators, such as an obvious brittle shear bands fabric (Fig. 4d, h). Along the road from Penas Negras to Gafarillios, these shear zones dip to the SW (Fig. 4a, b) and are sub-parallel to bedding in finer grained material (fine sands, silts and muds) that contain intercalated coarse sandstones and conglomerates. These zones contain small extensional duplexes with large sigma-shaped metres-size clasts, made up of more resistant sandstones and conglomerates, back-rotated and offset by synthetic Riedel shears (Fig. 4d, f, g, h).

One interesting geometry observed in outcrops is that of high-angle (70°–90°) fault segments developed in 0.15 m–4 m thick coarse sandstones (mostly granular debris flows) and conglomerates creating a staircase fault geometry by connecting layer sub-parallel (< 35°, but general layer parallel) segments in 0.05 m–0.4 cm thick fine sandstone, siltstones and mudstones bedsets (Fig. 5). Deformation along staircase faults is associated with cm-scale faults that have higher dips in the hanging-wall (40°–70°) than the footwall (20°–30°, Fig. 5). A direct relationship between the thickness of the underlying coarse sandstones and conglomerates and the overlying size of the step (or length of the flat) can be observed (Fig. 5h). Some faults do not display any apparent offset along individual steps, but the total displacement is obvious if the full stratigraphy is considered (Fig. 5). In more detail, some displacements along low offset faults are seen to be associated with layer parallel shearing and dragging in finer beds, shortcutting the steps by creating extensional horses (Fig. 5a–d). When displacement increases, these shortcutting features are less or not preserved (Fig. 5e, f, g). In other situations of staircase normal faults, we have observed a layer parallel shear confined to fine lithologies (Fig. 4d).

4.3. Implications for syn-kinematic basin infill and rheological control on the mechanics of normal faulting

Our field observations on bed thicknesses variation against normal faults and associated syn-kinematic wedges, together with intercalated chaotic packages of autochthonous material and intra-basinal clasts provide clear evidence for the link between sedimentation and normal faulting in the studied part of the Sorbas basin. The numerous syn-kinematic wedges provide an unusual strong age control of deformation, with the onset of extension and subsidence of the Sorbas Basin during late Serravallian-Tortonian times being associated with successive NW-SE and NE-SW oriented normal faults. Inversion must have post-dated the Tortonian in this part of the basin, since no contractional or transpressional structures of syn-kinematic character have been observed in any of the outcrop exposures of the Chozas Formation.

The clear differences in fault characteristics associated with differences in lithology demonstrate rheological control on the mechanics of normal faulting. In particular the high angle fault segments cutting through coarse sandstones and conglomerates and the low angle or layer parallel segments confined to fine lithologies imply a substantial contrast: the former must have been rheologically strong during

faulting, while the latter where rheologically weak.

Some ramp-flat geometries where steep segments in coarse layers are connected with each other via layer parallel segments (Fig. 4c, d, e) are best explained via two stages of faulting: first the formation of a high angle normal fault cutting through all layers, followed by layer parallel shearing creating offsets along steps in the normal fault. In other situations, the ramp-flat geometry is not affected by layer parallel shearing of finer sediments (Fig. 3e). Such geometries are also formed in response to the contrasting lithologies cross-cut by normal faulting, but the flattening of the fault segment is likely enhanced by the presence of unconsolidated sediments with high water content at the time of deformation (e.g., Childs et al., 2009). This mechanism cannot be applied to the staircase fault geometry where longer steep segments are connected via much shorter layer parallel segments (Fig. 5). In these situations, refraction during propagation of normal faulting (e.g., Childs et al., 1996; Schöpfer et al., 2006) is unlikely, because this does not explain the flat layer parallel segment of the staircase geometry. We infer that these staircase geometries formed by linking initially shorter Riedel shears or joints across rheologically weak layers in a vertical overlap shear zone, where the faults steps are connected upwards into the footwall across the overlap zone (e.g., Childs et al., 2009; Rykkelid and Fossen, 2002). This interpretation is supported by the synthetic rotation of sigmoidal clasts in the restraining vertical overlap structure. Alternatively, the staircase geometry may also have been formed as a result of growth and propagation of the faults nucleated within mechanically stronger layer and linked via weak layers (e.g., Gabrielsen et al., 2016). These faults were initially separated (i.e. soft-linked, e.g., Figs. 4c and 5a,b,c) and become connected when the fault offset exceeds the thickness of the weak layer (i.e. hard-linked, e.g., Fig. 5e, f, g).

5. The depositional environment associated with extension

The upper Serravallian–Tortonian sediments exposed in the SE part of the Sorbas Basin are characterized by coarse-grained clastics deposited in an alluvial fan and deltaic environment, which laterally changes to shallow marine and further to a deeper marine depositional system. These sediments were transported into the basin by a combination of rock-fall, stream flows and different types of gravity flows such as debris flows or high- and low-density turbiditic currents. The suspension fall-out deposition took place mainly in deltaic and deeper marine environments, often suppressed by gravity flows. Eighteen lithofacies were identified in the studied outcrops (Table 1). These lithofacies are organized in eight facies associations (Figs. 6–10), interpreted as alluvial, shallow marine, deltaic and deeper marine depositional systems.

Table 1
Lithofacies observed in the studied SW part of the Sorbas basin. Their interpretation follows a standard sedimentological procedure (Bouma et al., 1962; Postma, 1990; Miall, 1996; Talling et al., 2012).

Facies code	General description	Inferred depositional process
F1	Clast-supported; boulder to pebble conglomerate; with/without out-sized clasts; matrix: low amount of coarse-grained sandstone; subangular to subrounded clasts; poor to medium sorting; massive; plane base	Rapid sedimentation from cohesionless debris flow/granular flow
F2	Matrix-supported; cobble (boulder) to pebble conglomerate/sandstone; matrix: fine-grained sandstone/siltstone/mudstone; subangular to subrounded clasts; poor sorting; massive; planar base	Sedimentation from cohesive debris flow
F3	Clast- to matrix-supported; cobble to granula conglomerate/sandstone; moderate sorting; weak normal grading, imbrication; crude horizontal stratification; planar base	Longitudinal-bar or sieve deposits under subareal braided-stream flow
F4	Clast-supported; cobble to granula conglomerate; subangular to subrounded clasts; poor to medium sorting; normal grading; erosional base	Channel-lag deposits under subareal flashy braided-stream; sedimentation from subaqueous high-density turbidity flow
F5	Clast- to matrix-supported; cobble to granula conglomerate/sandstone; subrounded to rounded; weak sorting; planar crossbeds, imbrication; planar base	Transversal-bar deposits under subareal braided-stream; deltaic growths from older bar remnants
F6	Clast- to matrix-supported; pebble to cobble conglomerate/coarse- to fine-grained sandstone; subangular to subrounded; weak sorting; through crossbeds; graded or ungraded; erosional base	Channel fill under subareal braided-stream; sedimentation from high-density turbulent flow
F7	Coarse- to medium-grained (pebbly) sandstone; low matrix content; medium to well sorting; normal grading/massive; if presents mud rip-ups aligned; erosive/planar base	Rapid sedimentation from high-density turbidity currents (Ta division of Bouma et al., 1962)
F8	Medium- to fine-grained sandstone; parallel lamination; planar base	Sedimentation from subaerial sheet or stream flow; deposition from high- to low-density turbidity flow (Tb division of Bouma et al., 1962)
F9	Medium- to fine-sandstone; well sorting; ripple-cross lamination; climbing ripples	Sedimentation from sheet or stream flow; reworking of the sediments by wave action; deposition from low-density turbidity flow (Tc division of Bouma et al., 1962)
F10	Coarse- to medium-grained sandstone; no internal structure; often with scattered granulas, pebbles	Sedimentation from subareal to subaqueous cohesionless debris flow
F11	Medium- to fine-grained sandstone; moderate sorting; planar crossbeds; planar base	Sedimentation under sheet or stream flow; deposition from unidirectional, steady high-density turbidity currents
F12	Medium- to fine-grained sandstones; well sorting; weak normally graded/ungraded; low-angle crossbeds; planar base	Dunes (lower flow regime) under subareal sheet flow or stream flow; deposition from wave and/or tidal currents passing through channel; lateral accretion
F13	Fine-grained sandstone interbedded with siltstone; sometimes with scattered granulas; laminated or massive; planar base	Sedimentation from suspension of waning floods; suspension fall-out in local overbank flood areas or abundant channel; sedimentation from low-density turbidity flow (Td division of Bouma et al., 1962)
F14	Fine-grained siltstone to mudstone; planar lamination or massive	Sedimentation from waning low-density turbidity flow (Te division of Bouma et al., 1962) or cohesionless density flow
F15	Grey mudstone; massive/weak planar lamination	Particles settling from water column
F16	Yellow marl; massive/weak planar lamination	Particles settling from water column
F17	Fine-grained sandstones, structureless	Bioturbated sandstone
F18	Coarse- to medium-grained sandstones; chaotic; scattered pebbles, mud rip-ups	Slump deposit

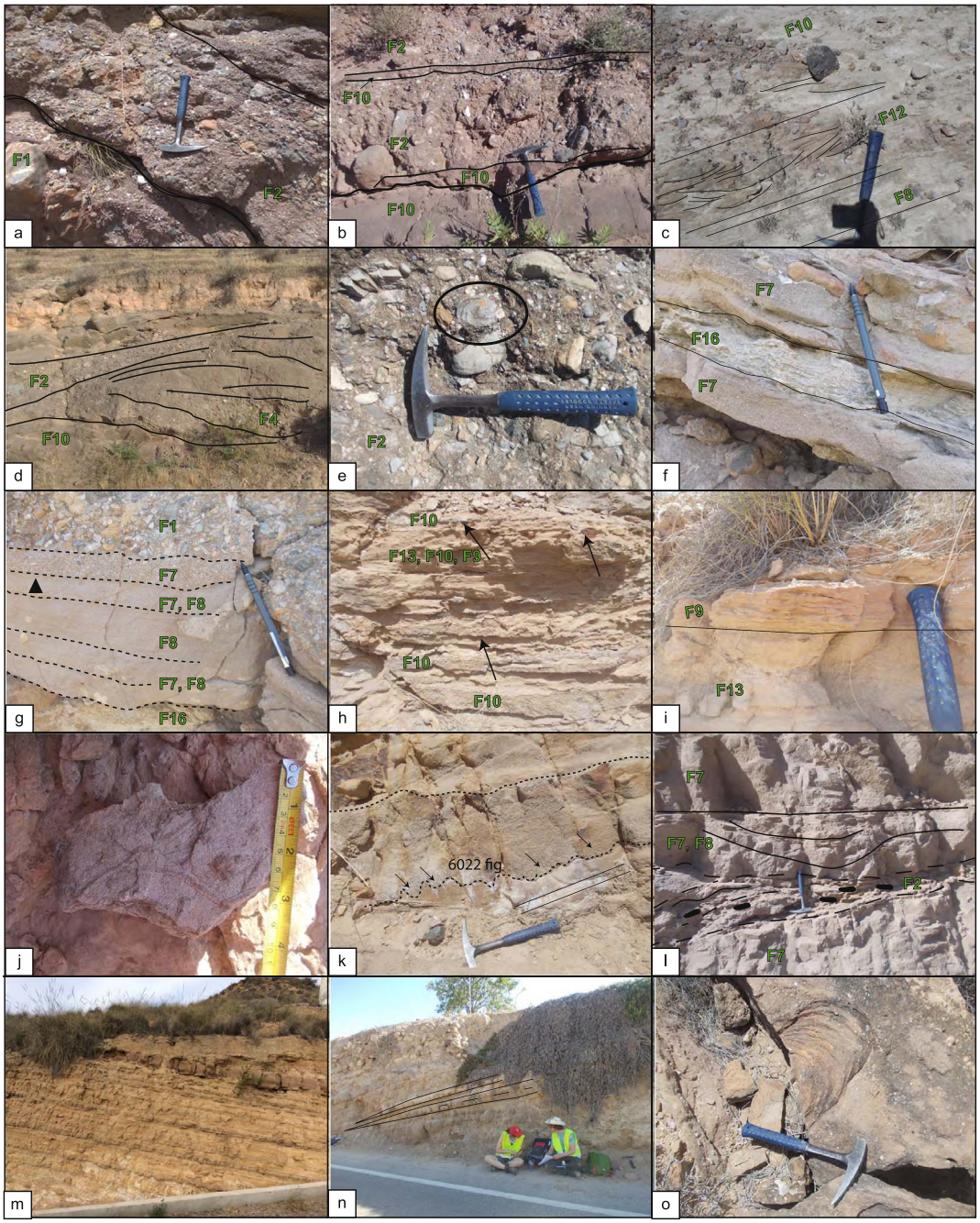

Fig. 6. Typical examples of the main facies associations. See Table 1 for facies details and Fig. 1c for photo locations. a) facies association A1 with matrix- to clast-supported conglomerates deposited in a proximal alluvial fan environment. Thick black line marks the bedding; b) facies association A2 with structure-less sandstones and conglomerates deposited in a distal alluvial fan environment; c) facies association B with well sorted mature yellow trough cross bedded sandstones deposited in a shallow water marine (shoreface) environment; d) facies association C1 with channelized delta plain deposits; e) facies association C2 with sheet-like polimict conglomerates deposited in a river-dominated delta front environment. Note the oyster shell inside the black ellipse; f) facies association C2 with coarse-grained sandstones containing isolated out-sized clasts intercalated with wavy laminated yellow carbonate mudstone deposited from subaqueous distributary channels and mouth bars affected by a wave and tidal influence; g) facies association C2 with amalgamated sandstones deposited from high-density turbidity currents capped with granular flow deposit in the delta front environment. Dashed lines delineate bed sub-units; h) facies association C3 with burrows in sandstones and mudstones interrupted with pebble to granula clastic episodes; i) facies association C3 with ripple-cross laminated sandstone and bioturbated sandy mudstones deposited in a prodelta settings; j) facies association C3 with horizontal burrows in prodelta sandstones; k) facies association C4 with amalgamated event beds comprised of an alternation of granula sandstones and clast- to matrix-supported conglomerates, whereas the base of the latter is characterized by loading structures (black arrows); l) facies association C4 with interference of amalgamated beds and lateral channels (likely fault perpendicular flow); m) facies association C5 with parallel laminites, siltstones and mudstones deposited on the basin plain; n) isolated medium-grained sandstone lobes deposited from high-density turbidity currents in terminal lobes, and; o) Zoophycos in distal submarine fan environment. (For interpretation of the references to color in this figure legend, the reader is referred to the web version of this article.)

5.1. Alluvial fan and shallow marine systems

The alluvial system crops out in a restricted part of the basin (north of Gafarillos village, Fig. 1c) and is made up by red multi-storey bodies displaying sheet-like geometry. The flow was often confined by coeval normal faults, which created centimetres to metres wedge-shaped geometries by thickening towards the fault (Fig. 10a).

Facies association A1 is characterized dominantly by thick-bedded (0.5–2 m) pebble to cobble conglomerates and coarse-grained sandstones (F1, F2 less common F10, Table 1, Fig. 6a). They are poorly sorted and immature, and contain a large compositional diversity of clasts (such as quartzite, schists, dolomites, marble, recycled conglomerates and sandstones). The base is planar with small scale erosional relief (< 10 cm). These dominant lithologies alternate with thin-bedded (< 0.1 m) fine-grained sandstones and siltstones (F9, F13, Table 1). This facies association unconformably overlies the pre-Miocene basement and is gradually replaced by facies association A2(see below).

Facies association A1 is interpreted as a proximal alluvial fan system dominated by deposition of debris flows (e.g., Nemec and Steel, 1984; Blair and McPherson, 1994). The angularity and lithological nature of the clasts derived from the surrounding metamorphic basement suggest a proximal source area located in the neighbouring sierras. The clasts derived by eroding the fault scarp indicate that these flows originated from remobilization of colluvial rock-fall deposits at the base of an active fault (e.g., Blikra and Nemec, 1998; Longhitano et al., 2015).

Facies association A2 is characterized by medium-bedded (0.2–1.2 m) sand prone deposits (F2, F3, F7, F8, F10, less common F4, F5, Table 1, Fig. 6b). These deposits are often channels filled with pebble to cobble conglomerates with erosive base and gradational top. The imbrication and plane cross-bedding indicate a SW-wards flow direction. The sandstones are often interbedded with finer deposits (F9, F11, F13, Table 1). This facies association grade into facies association C1 (see below).

Facies association A2 is interpreted as deposition in a medial to distal alluvial fan environment dominated by flood-related braided flows alternating with debris flows (e.g., Nemec and Postma, 1993; Barrier et al., 2010). Finer clastics were deposited by combined waning flows and suspension in a lower energy environment. The cross-stratified bed sets and channels with erosive base resulted from migration of

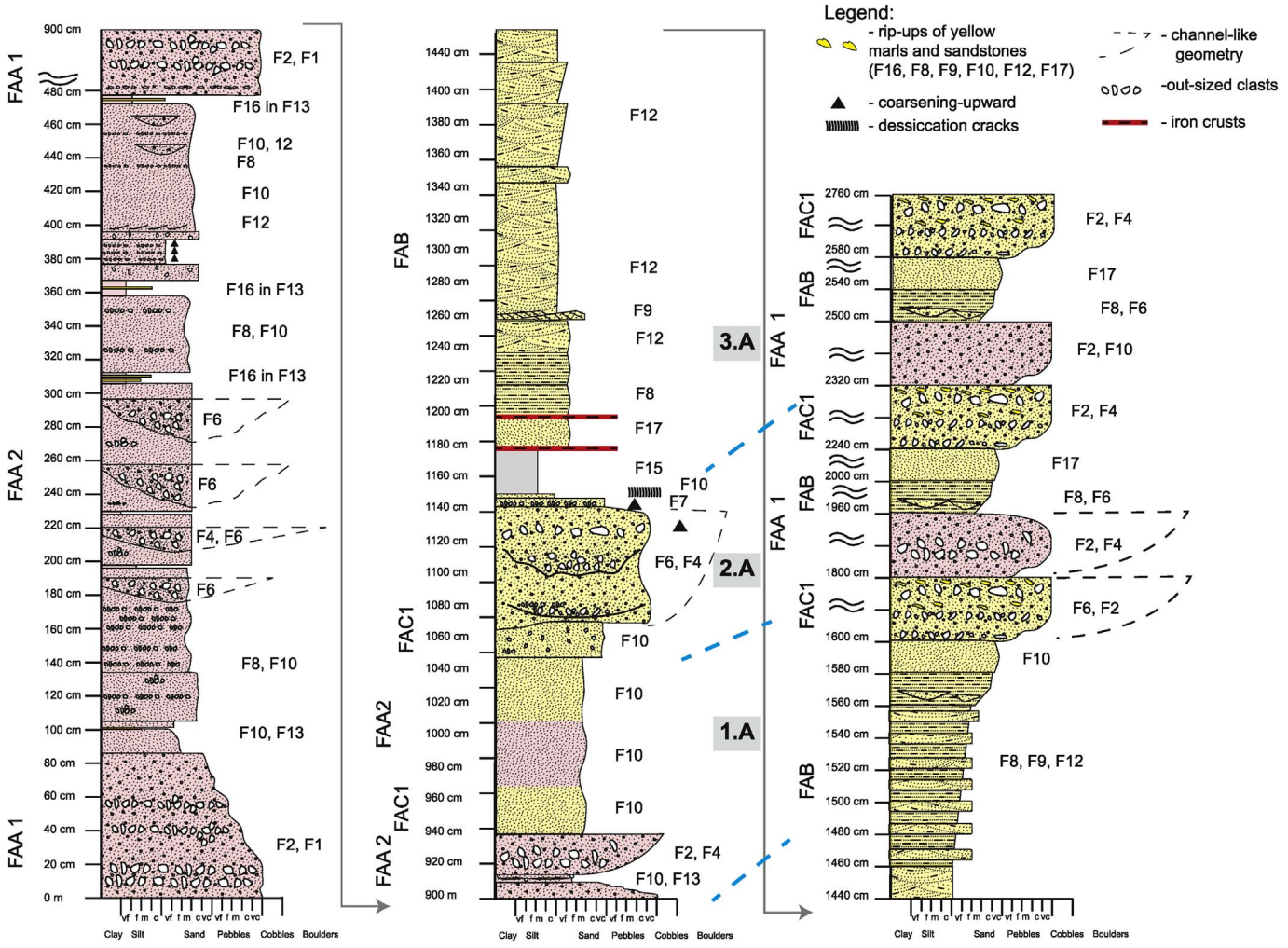

Fig. 7. A detailed sedimentary log of the alluvial to shallow water marine environment transition observed in the SE part of the Sorbas Basin. See Table 1 for facies details and Fig. 1c for log location. FAA1 and FAA2 – facies association A1 and A2, respectively; FAB - facies association B; FAC1 - facies association C1. The grey rectangles with numbers represent stages of fault activity: 1 - high displacement rates; 2 - gradual termination of the faulting activity, and 3 - fault quiescence.

small distributary channels within a fan system (e.g., Blair and McPherson, 1994).

Facies association B is characterized dominantly by tabular medium-bedded (0.05–0.4 m) well sorted yellow calcareous sandstones (F8, F9, F12, F17 and minor F10, Table 1, Fig. 6c). These sandstones may be structure-less or contain climbing-ripples and trough-cross bedding, often draped by mud. Parallel and ripple-cross lamination is less obvious. Beds are separated by thinly-bedded (0.01–0.15 m) mudstone layers (F15, Table 1). Towards the top, this facies association becomes locally pebbly with strings or isolated outsize clasts. This facies association shows a general coarsening-upwards trend and is deposited beneath or lateral from to delta deposits (i.e. delta channel, C1, see below).

Facies association B is interpreted as shallow marine deposits with low or no fluvial influence. Mudstone drapes suggest periods of quiescence and deposition from suspension. The relative good sorting and lack of coarser-grained material in the lower part of the succession suggest low clastic sourcing and reworking (e.g., Carr et al., 2003). In the upper part of the coarsening upwards sequence, the occurrence of outsized clasts and pebbly strings infers a higher proximal clastic influx (e.g. Young et al., 2000).

5.2. Deltaic system

Facies association C1 is characterized by thick-bedded (0.7–1.5 m) conglomerates and sandstones (F2, F4, F6, F10, F17, minor F3, Table 1, Fig. 6d). The individual bed geometry varies from wide channels with erosive base and rip-ups of underlying fine sandstones and marls, to less frequent sheet like layers with planar base. They include shell fragments (Pectens, oysters, < 5%). This facies association alternate with facies associations A and B by building coarsening-upward successions (Fig. 7). The contact with facies association B is gradual (over ~1 m), while the contact with facies association A is sharp.

Facies association C1 is interpreted to be deposited from high energy hyperpycnal and debris flows based on the presence of channels, rip-ups fragments and a general coarsening-upward trend. These sedimentary features are typical for deposition at the mouth of river-dominated deltas (i.e. delta plain, e.g., García-García et al., 2006).

Facies association C2 is characterized by an alternation of thick-bedded conglomerates and sandstones (0.2–2 m) (F1, F2, F7, F8, F10, Table 1, Fig. 6e, f, g), and thinly-bedded (0,1 m to 0,2 m) yellow marls (F16, Table 1, Fig. 6f). The sandstone and conglomerate beds have generally a sheet-like amalgamated geometry, in which the amount of matrix and grain-size varies both vertically and laterally. The amalgamated beds may be up to 8 m thick. Bed bases are plane to slightly erosional. The conglomerates show high textural maturity and roundness and may be imbricated. Most sandstones are normally graded and contain a variety of sedimentary structures, such as parallel lamination, climbing ripples, flaser lamination and ripple cross-lamination. They also contain shell fragments (Pectens, oysters, < 5%). Occasionally, sandstones are structure-less with floating clasts or pebble to cobble strings. Well rounded outsized clasts (up to 1 m) are common. This facies association passes into facies association C1 upslope and C3 downslope. This association commonly forms upward coarsening units of tens of metres.

Facies association C2 is interpreted to be the result of deposition from concentrated, high-energy flows (dominated by debris flows and granular flows where turbulent flows are less common) during high discharge episodes in delta front environment (e.g., Young et al., 2000; Schomacker et al., 2010). These flow episodes are separated by periods of low discharge that allow sediment redistribution and reworking by waves and tides, and colonization and bioturbation (e.g., Dabrio, 1990; Aschoff et al., 2016). Relatively small bedset thicknesses indicate deposition in shallow water environment (~10's of metres of water), where the absence of clinoforms suggests deposition in a coarse-grained shoal water type of the fan delta (e.g., Lewis et al., 2015; Postma, 1990).

Facies association C3 is characterized by alternation of thin-bedded (0.01 m to 0.15 m) medium- to fine-grained sandstones, siltstones, mudstones and marlstones (F7, F8, F9, F13, F16, F17, Table 1, Fig. 6h, i, j). Individual beds have a sharp planar base. The medium- to fine-grained sandstones are well sorted and, usually show ripple-cross lamination (climbing, symmetric and asymmetric), wave ripples and horizontal lamination (Fig. 6i). These sandstones have rare convolution or hummocky lamination and locally contain burrows and plant material (Fig. 6j). Near the transition with facies association C2, these sandstones may contain floating clasts or strings.

Facies association C3 is interpreted to be deposited in a low energy prodelta environment, with periodic low- and high-density turbidity currents derived from a continental source (e.g., Mulder and Alexander, 2001; García-García et al., 2011). The rare hummocky bedforms indicate an influence of storm waves due to either combined flows (waves and currents) or complex oscillatory flows (e.g., Arnott and Southard, 1990). The presence of benthic organisms (i.e. vertical and horizontal burrows, Skolithos) together with wave and tide generated sedimentary structures indicate deposition above fair-weather wave base in sublittoral zone (e.g., Aschoff et al., 2016).

5.3. Deeper marine system

Facies association C4 is characterized by an alternation of a tabular and wedge shaped thick-bedded (0.5–1.2 m) facies dominated by sandstones and conglomerates (F7, F8, F18, occasionally F1 and F2, Table 1, Fig. 6k, l) and medium to thick-bedded (0.1–1 m) fine-sandstone and siltstone facies (F8, F9, F13, Table 1). The base of individual beds is sharp and, in some places, loading is present. Locally, this association contains wide scours with erosional base and granular/pebble lags and rip-ups (Fig. 6l). Sandstone-rich beds are often stacked, which creates 4–8 m thick units (Fig. 8). Bedding planes within these units are represented by aligned mud rip-ups, shells and/or grain-size breaks. Water escape structures, sand injections and mud rip-ups are common (hybrid beds, H1 division of Haughton et al., 2009). The fine-sandstones/siltstones include up to 40 cm thick hybrid beds with an upper banded part (H2 division of Haughton et al., 2009). This banding is produced by monotonous variations in the clay matrix of the sandstones. Sandstones are structure-less or may show parallel lamination. The succession is organized in coarsening- (and fining-) upward sequences that alternate vertically and laterally with facies association C5 (Fig. 8).

Facies association C4 is interpreted to be the result of rapid deposition from high density turbidity and debris flows at high aggradation rates, deposited on the lower part of the slope and axial part of proximal submarine lobes (e.g., Kneller and Branney, 1995; Prélat et al., 2009; Talling et al., 2012). Unusually, thick coarse-grained sandstone and fine-grained sandstones/siltstones are deposited from hybrid flows showing evidence of flow transformation from poor to more cohesive flows and their coexistence with turbidity flow (e.g., Haughton et al., 2009). The fine sandstone/siltstone unit suggests deposition from dilute turbidity currents and hybrid flows outside the main lobe (off-axis or fringes, e.g., Prélat et al., 2009). The presence of boulders and slumps indicate slope steepening (e.g. Blair and McPherson, 1994).

Facies association C5 is characterized by thin bedded (0.01–0.1 m) heterolithic packages of mudstones, siltstones, fine thin sandstones (F13, F14, F15, Table 1, Fig. 6m, n, o) intercalated with fine- to medium-grained sandstones (F7, F8 and F9, Table 1). Bedding is

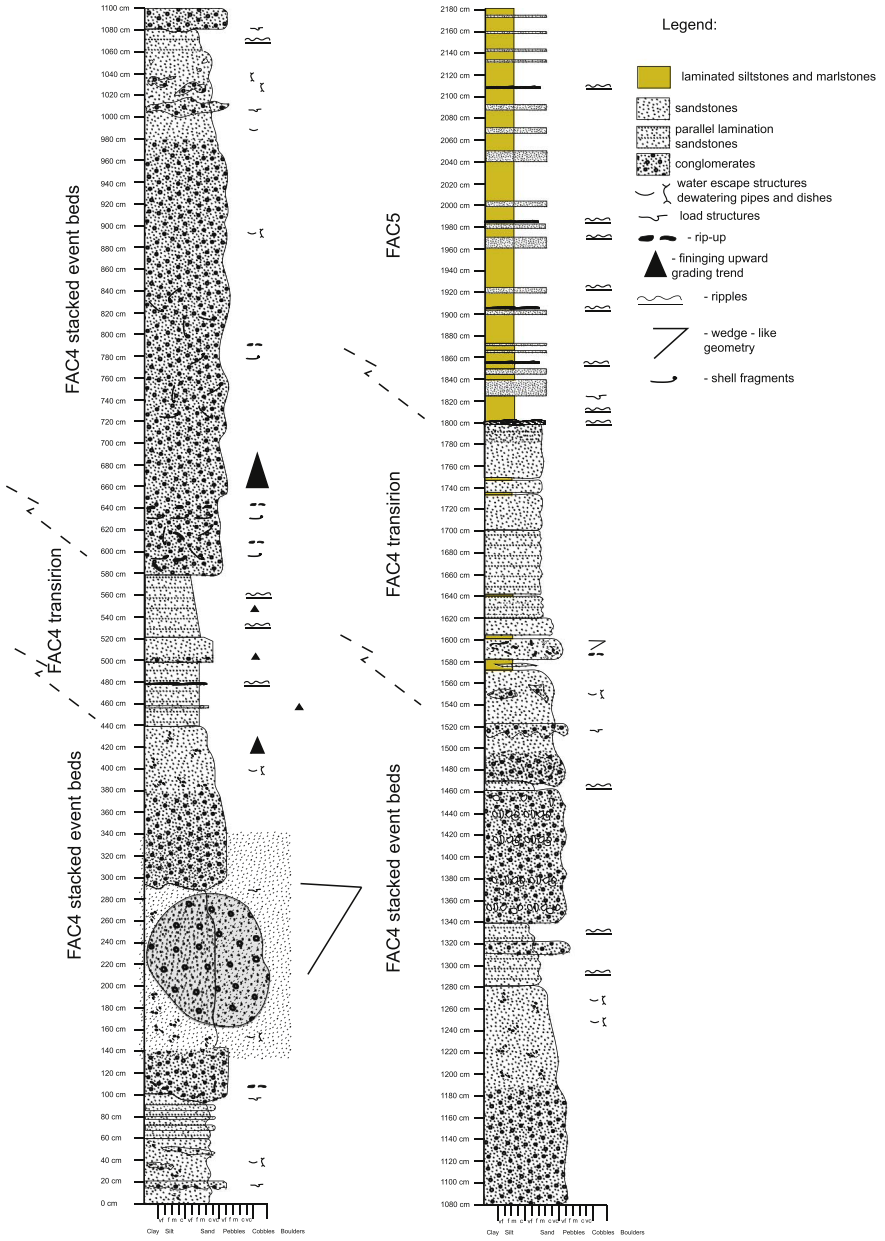

Fig. 8. Detailed sedimentary log of a prograding submarine-fan into the basin plain environment in the SE part of the Sorbas Basin. See Fig. 1c for log location. FAC4 - facies association C4; FAC5 - facies association C5.

marked by sharp vertical alternations of dark yellow and light grey beds, on a mm to cm scale. Sandstone (0.1–0.2 m thick) intercalations divide this monotonous succession into packages of variable thickness (0.1–0.9 m). Beds are continuous tabular to lobate. Scours are rare and associated with medium- to coarse-grained sandstones (Fig. 9f). Thicker and coarser sandstone layers occur more frequently in close proximity (within 1–2 m) to proximal submarine fan facies association (C4). This facies association is commonly observed as tens of metres' thick intervals occasionally interrupted by chaotically deformed packages of autochthonous material (up to 2 m thick) or sandstones (F18, Table 1, Figs. 3e, f and 9a). Deformed packages include folded heterolithic beds and rip-ups enclosed in a poorly sorted silty/sandy matrix and have sharp to erosive contacts with the adjacent undeformed heterolithic packages. This chaotic facies is associated with normal faults up slope and reverse fault down slope.

Facies association C5 is interpreted as a product of combined deposition from dilute turbidity currents and suspension fallout in a distal submarine fan environment over the basin plain (e.g., Bouma et al., 1962; Talling et al., 2012). Planar, climbing-ripple and ripple lamination resulted from bed tractional reworking under moderate to high aggradation rate (e.g., Southard, 1991; Mutti, 1992; Talling et al., 2012). Isolated sandstone beds represent the expression of the distal-most progradation of high density turbidity flows bypassing the lobe environment (e.g., Talling et al., 2012; Stevenson et al., 2015). The intercalated chaotic packages suggest syn-depositional deformation due to remobilization of autochthonous intra-basinal material (e.g., Spychala et al., 2017). When combined with normal faults up slope and reverse faults downslope, this facies association shows periods of gravitational sliding, i.e. toe slope decollements (e.g., Postma, 1984).

5.4. Sedimentological events during deposition

We use the term ‘event-bed’ in the sense of a depositional event characterized by contrasting lithologies that reflects the stacking of one or multiple flow types, which does not necessarily mean that beds are isolated or unusually thick. Such event beds are rather frequent in the

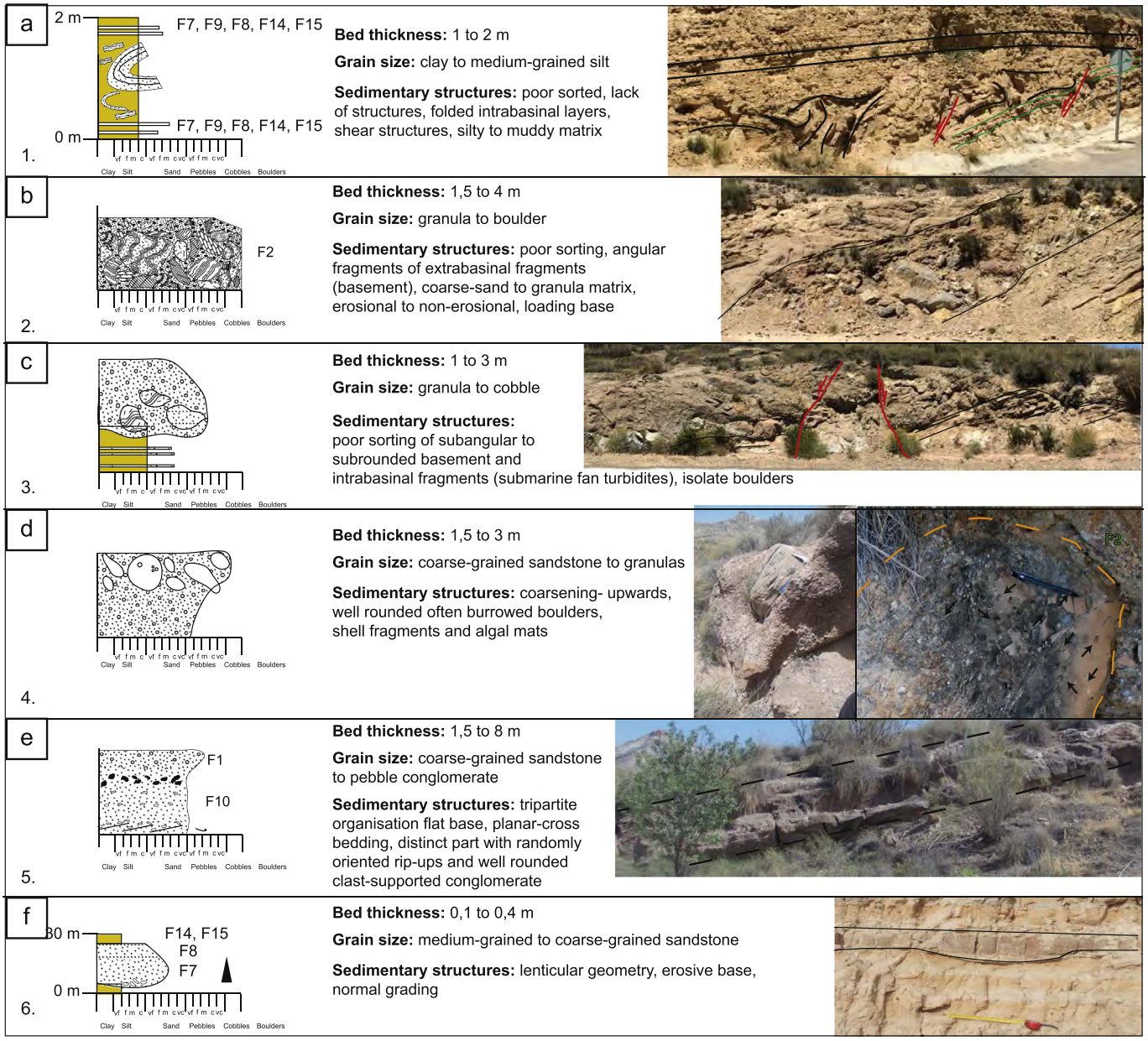

Fig. 9. Typical examples of event beds. See Table 1 for facies details and Fig. 1c for photo locations. a) event bed type 1 that resulted from seismically triggered slope collapse, leading to remobilization and embedding of intra-basinal layers and clasts within a distal submarine fan environment (facies association C5); b) event bed type 2 that resulted from uplift and erosion of the footwall, leading to direct delivery of extra-basinal material into a distal submarine fan environment by debris flows; c) event bed type 3 that resulted from slope failure due to activity of intra-formational faults; d) event bed type 4 deposited from debris flows that provided the main way to re-deposit material from shallow environment further into the basin; e) event bed type 5 that resulted from debris flow partitioning along its long transport trajectory, and; f) event bed type 6 formed as isolated distributary channels within a distal submarine fan environment.

studied sedimentary succession (Fig. 9). Near the source area, these beds are observed as thick packages of proximal alluvial fan deposits deposited over distal alluvial or deltaic sediments (Fig. 7). The rapid transition of facies associations, and the angularity and nature of the clasts suggest that normal sedimentation was interrupted by moments of rapid uplift and erosion of normal fault footwall scarps and sedimentation in their proximity (e.g. Longhitano et al., 2015). In more distal marine environment, six types of event beds can be identified on the basis of clear contrast in sedimentation.

Event bed type 1 is characterized by chaotically deformed (i.e. folded, bed raft, rip-ups, Fig. 9a) thin bedded heterolithic packages enclosed within a poorly sorted silt to clay matrix. These beds have sharp upper and lower boundaries. They occur within the distal submarine fan facies association C5 and reach 2 m in thickness. Deformation in such packages is often connected with a decollement to a break-up zone made up by normal faults, while frequent isolated rafts affected by thrusts or normal faults are observed in the field (Fig. 3e, left part and f). In some instances, the close association with normal faulting is observed by the decollement starting at these faults in their syn-kinematic deposits.

Event bed type 1 is interpreted as a toe-slope decollement created by gravitational sliding which evolved into debris flow along the depositional slope on the way to the submarine fan environment (e.g., Talling et al., 2012). In such an environment, slides and debris flows could be initiated by intra-basinal slope steepening, liquefaction of underlying mud-rich deposits and/or failure generated by overpressure due to high sedimentation rate on the slope (e.g., Gee et al., 1999; Bull et al., 2009). In our case, the frequent association with syn-depositional normal faults

demonstrates that sliding is driven by tectonics. These event beds were most likely triggered by fault induced seismicity (e.g., Bugge et al., 1988; Spychala et al., 2017), similar to what has been previously discussed in the neighbouring Tabernas Basin (such as the "Gordo megabed" of Kleverlaan, 1987). However, when compared with the large-scale chaotic mega-beds in this basin, our type 1 events are much smaller in size and do not appear to have a basin-wide continuity.

Event bed type 2 is characterized by angular out-sized extra-basinal clasts (up to 2 m) enclosed within poorly sorted sandy matrix (Fig. 9b). Beds are often isolated and interbedded within relatively finer layers which show abundant water escape structures. Event bed type 2 is observed in the apical parts of coarsening-upward sequences deposited in the proximal part of the submarine fan deposits (Fig. 11a, b; see also the Supplementary material).

Event bed type 2 is interpreted as a result of rapid deposition from land-derived debris flows bypassing the shallow water and slope, and depositing the material at the toe of the slope. The character of the beds (oversized angular extra-basinal clasts) indicates that these flows were generated in an alluvial environment by remobilization of rock-fall material eroded from the uplifted footwall of the basin bounding fault and rapidly deposited at the base of the slope during high-discharge events (e.g. Leppard and Gawthorpe, 2006; Strachan et al., 2013).

Event bed type 3 is characterized by a bipartite organization. The lower part consists of sandy matrix supported outsized clasts, of both extra-basinal (dolomites, schists, marbles) and intra-basinal (medium- to coarse-grained turbidites) origin. The upper part is composed of structure-less sandstones (Fig. 9c).

Event bed type 3 is interpreted to reflect cohesion-less debris flow deposition that was followed by high-density turbidites deposited as part of the same general waning event (e.g. Talling et al., 2012). The intra-basinal clasts resulted from footwall uplift and degradation of normal faults, shedding material towards the distal submarine fan environment. Faulting caused coeval slope instability, leading to remobilization of reworked extra-basinal clasts that are mixed with the intra-basinal material along the slope on the way to the distal submarine fan environment. Intra-basinal normal faults localized the gravity flows on the basin plain (Fig. 9c).

Event bed type 4 is characterized by out-sized well rounded cobbles and boulders of extra-basinal clasts (dolomites, schists, marbles), with some dolomite clasts containing lithophaga borings (Fig. 9d). They show a bipartite organization with a matrix-supported pebbly sandstone that is coarsening-upwards to a cobble-boulder conglomerate.

Event bed type 4 is interpreted to result from the redistribution of avalanching material along an unstable slope (e.g., Postma, 1984). Frequent borings suggest storage and reworking of the material from a delta plain or beach environment before re-deposition further into the basin (e.g., Puga-Bernabéu et al., 2007a, 2007b; Lewis et al., 2015). The remobilization of material stored in the shallow water environment can be induced by seismically triggered slope failure or high fluvial discharge (e.g., Haughton et al., 2009; García-García et al., 2011).

Event bed type 5 is characterized by a tripartite organization (Fig. 9e). The lower part of the event bed may include planar cross-bedding formed by alternating matrix-supported conglomerates and pebbly sandstones flat bands (F1, F2, F10, Table 1). The middle part of the bed is composed of sandstones with silt to clay matrix and narrow zones of randomly oriented marl (often yellow) rip-ups and scattered pebbles. The upper part is made up of a clast-supported conglomerate.

Event bed type 5 is interpreted to result of partitioning of a debris flow along the slope (hybrid flow, e.g. Haughton et al., 2003; Kane and Pontén, 2012). Our observations suggest that the debris flow may transform partially into an independent forerunner of a turbidity current along its long transport pathway (i.e. long transport far into the basin, e.g., Haughton et al., 2003; Haughton et al., 2009). During transport, the turbidity current decelerates and becomes diluted enough to develop planar cross-bedding at the base of the event beds (Fig. 9e). Similar bed types (i.e. turbidites linked with debrites) are common in distal and lateral margins of deep water systems caused by failure of a syn-tectonic slope (e.g., syn-rift Jurassic submarine fans of the North Sea Basin, Haughton et al., 2003). This scenario is inferred by extra-basinal components and rip-ups of shallow water marls.

Event bed type 6 is characterized by isolated medium- to coarse-grained sandstones interbedded within the finer distal submarine fan facies association C5 (Fig. 9f). This event bed has often a wide scour, is granular at the base, has a general coarsening-upwards pattern and contains climbing ripple-cross lamination. Such beds are observed in the vertical succession as part of coarsening- or fining-upward successions, but cannot be clearly ascribed to any of these patterns.

Event bed type 6 is interpreted as an episodic influx of land-derived material into a distal submarine fan environment. The material was transported along a distal terminal lobe, most likely derived from turbidity currents originating from concentrated hyperpycnal flows during high discharge (e.g. García-García et al., 2011). The beds are thus likely related to high discharge events during wet seasons and shows no link to tectonic activity, i.e. uplift and/or erosion prior to remobilization and deposition.

5.5. Syn-kinematic sedimentation

Clear syn-kinematic deposition is observed in sedimentary wedges deposited against normal faults and sealed by finer grain sediments. As a function of the direction of normal faulting and the related orientation of the slope along which sediments were supplied to the basin, we distinguished two types of syn-kinematic wedges: synthetic (same direction) and antithetic (opposite direction). This means that synthetic wedges are composed of terrestrial material transported across or along the slope created by the normal faults footwall, while antithetic wedges consists of terrestrial material transported along a slope created by antithetic tilting of the hanging-wall of normal faults. Both synthetic and antithetic wedges thicken towards the fault and pinch out in the hanging wall direction, but are oriented differently relative to source area, i.e. they thicken SW-wards and NE-wards, respectively. Both are locally observed to be associated with footwall uplift and erosion.

In the alluvial and deltaic parts of the succession, synthetic wedges are controlled by centimetres to decimetres offset of low- and high-angle normal faults (Fig. 10a–c), while antithetic wedges are less common. These wedges contain matrix-supported (cobble to pebble) sandstones and conglomerates that often have outsized clasts derived from cohesive debris flows (F2, Table 1, Fig. 10a–c). These observations show rapid deposition driven by the instability of a syn-tectonic slope. An increase in mud content enhances the flow strength, which enables the transport of out-sized clasts (e.g., Talling et al., 2012). The interbedding or sealing of wedges with finer clastic sediments is interpreted to result from diluted or waning turbidity currents and/or suspension fall out during moments of tectonic quiescence (F14, F15, F16, Table 1). Rapid changes in sedimentary facies across these wedges reveal locally forced progradation of more proximal (higher energy) over distal (lower energy) facies, driven by the activity of normal faults. However, these faults may confine distributary channels and influence the lateral migration of the fan system.

A large number of synthetic and antithetic wedges were observed in the marine part of the succession (Figs. 3a, b and 10d, e). Some of these wedges illustrate a rapid transition from a distal to proximal position even at the scale of a single bed or bed set (Fig. 10e). Such wedges are made up of debris flow and high-density turbiditic flow deposits. More complex, larger scale antithetic wedgescontaining several syn-kinematic layers are related to large offset ramp-flat normal fault systems (Fig. 3a, b). Several simultaneous wedges with variable ramp offsets are associated with a coarse influx of debris flows, which is sealed by finer grained lithologies in the overall submarine fan environment (Fig. 3a, b). Successive offsets along these faults are clearly associated with high-frequency sedimentary patterns, which are otherwise very similar in expression as autogenic cyclicity created by submarine lobe shifting,

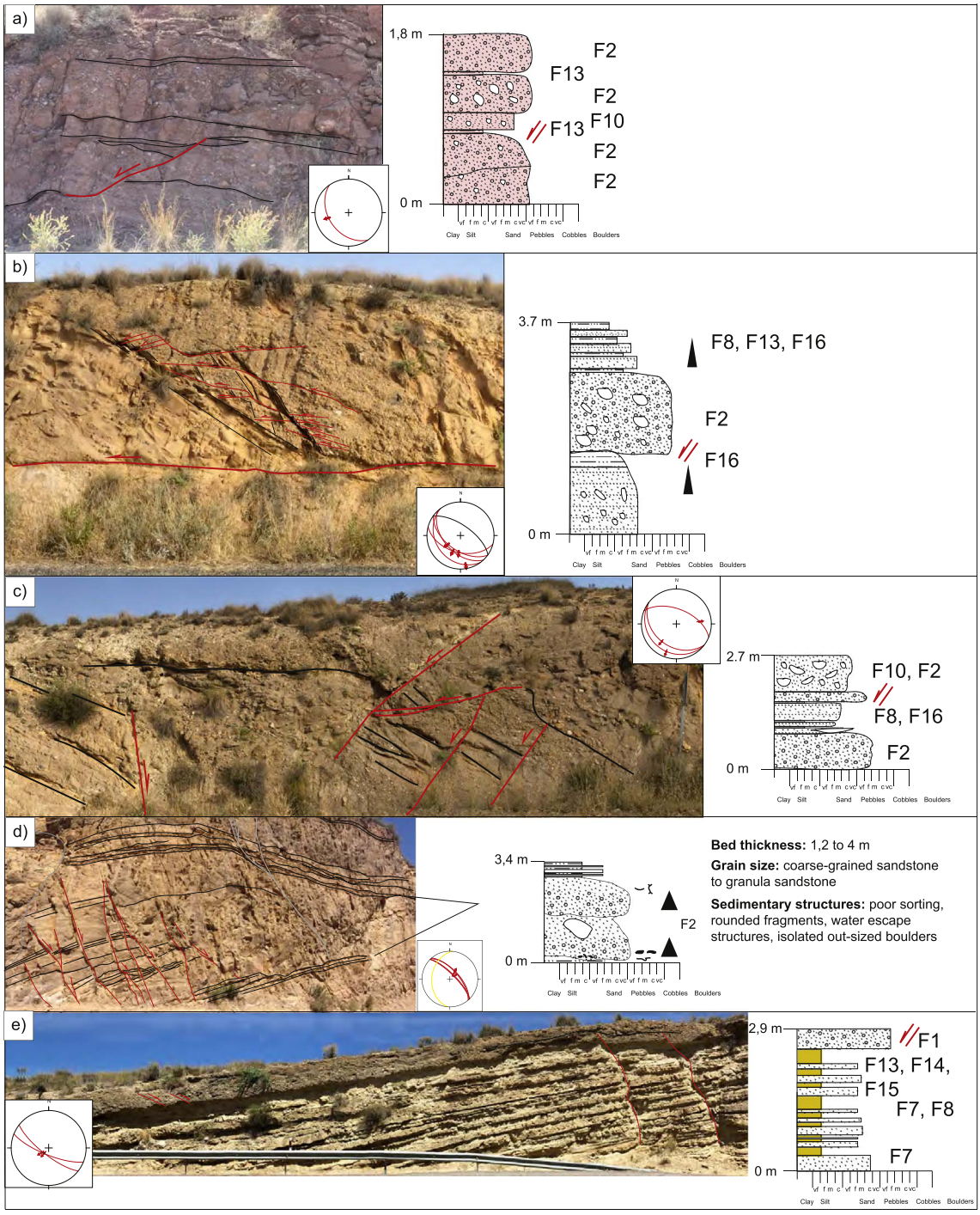

Fig. 10. Typical examples of syn-kinematic wedges associated with normal faults. See Table 1 for facies details and Fig. 1c for photo locations. a) Syn-kinematic wedges developed in a distal alluvial environment associated with synthetic normal faulting; b) syn-kinematic wedges developed in a delta front environment associated with synthetic normal faulting; c) syn-depositional domino-type normal faults triggering deposition of matrix-supported sandstones in a delta plain environment; d) syn-kinematic wedge that is controlled by antithetic rotation of the hanging-wall during faulting in a submarine fan environment, and; e) a coarse-grained debris flow event confined by the activity of normal faults in a distal submarine fan environment.

driven by migration or instability of distributary channels (e.g., Prélat et al., 2009).

6. Discussion

Our data show a direct relationship between deformation and deposition of syn-kinematic wedges in the hanging-wall of normal faults during the onset of basin formation (e.g., Fig. 10). Furthermore, the studied upper Serravallian-Tortonian sediments of the Sorbas basin are organized in two different orders of deposition driven by tectonic activity. The higher order of tectonically induced cycles (or sedimentary successions) are deposited during short-termed perturbation of the depositional system created by the onset of normal faulting and/or changes in the slip-rates along the normal faults. Such perturbations create up to 20 m thick coarsening- and fining-upward packages (e.g., Fig. 11b). In the studied succession, we have observed 5 such episodes of cyclic sedimentation, every time associated with the onset or acceleration of normal faulting (see also Supplementary material). The lower

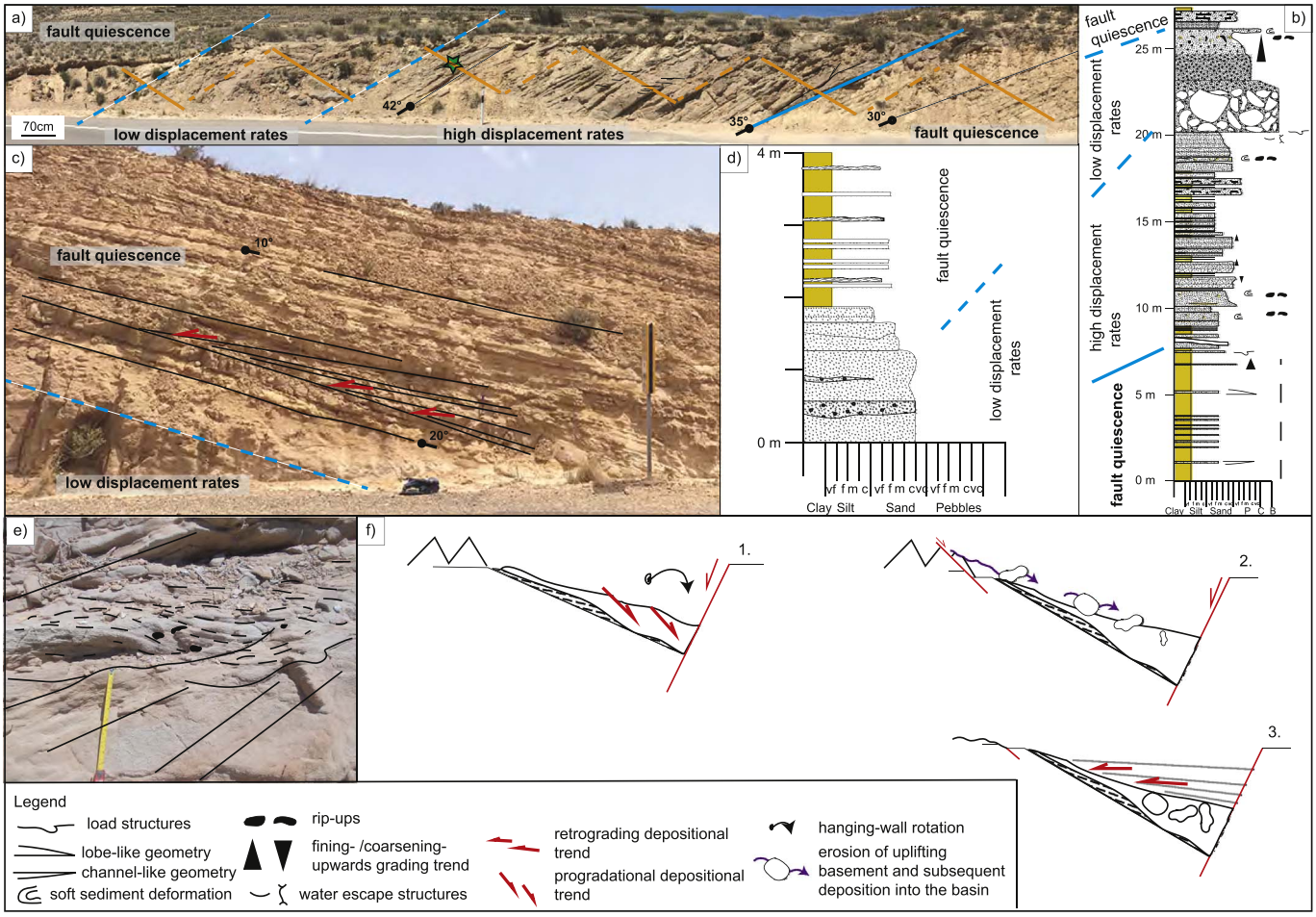

Fig. 11. Field examples of deposition controlled by slope steepening and shallowing, illustrating the concepts of system tracts formed during high- and low-displacement rates along normal faults, as well as during tectonic quiescence. See Fig. 1c for photos location. a) Coarsening-upward succession reflecting the overall progradational and aggradational depositional trend at the toe of the slope, formed during slope steepening to > 10°. The orange lines mark the location of the sedimentary log in b. The thick blue line marks the base of the sequence controlled by normal faulting. Dashed blue lines mark the separation between system tracts. Green star represents the position of backsets in e; b) detailed sedimentary log of the coarsening-upward succession seen in a; c) retrogradational depositional trend following slope shallowing and exhaustion of source area formed during the transition from the low displacement rate to tectonic quiescence system tracts. Red arrows indicate aggradational onlapping geometry (1. 5 m high traffic sign for scale); d) detailed sedimentary log showing fining upward succession deposited during gradual termination of fault activity and subsequent slope shallowing; e) inset of a showing scour fill with up dip sigmoidal backset stratification formed due to hydraulic jump (20 cm long measuring tape for scale). Black dashed line indicates the sigmoidal stratification. Black thick line shows the background bedding; f) interpretative sketches showing sedimentary response to hanging-wall antithetic rotation during three main stage of fault activity that separate individual system tracts controlled by tectonics: 1 - high displacement rates; 2 - low displacement rates, and 3 - fault quiescence. (For interpretation of the references to color in this figure legend, the reader is referred to the web version of this article.)

order tectonically induced cycles (or sedimentary successions) are deposited during long-term perturbations of the depositional system as a consequence of the overall migration of deformation and faulting during basin formation and evolution. These cycles create major changes in the depositional environment during the transition from continental to deep-marine sedimentation. Different orders of deposition have been observed in many sedimentary basins around the world, either at high-order (such as the Wollaston Forleand Group in east Greenland or the Suez Rift, Henstra et al., 2016; Strachan et al., 2013), or at low-order (such Sarajevo-Zenica Basin of the Dinarides, Andrić et al., 2017).

Other external forcing factors are less or not observed in the studied sedimentary successions. For instance, the eustatic sea level drop of ~50 m that took place at ~11–9 Ma (Miller et al., 2005) is not visible in deposition and appears to be suppressed by tectonic subsidence and rapid deepening of the basin. Such observations are commonly observed in tectonic active extensional basins, such as during the deposition of the middle Jurassic Hugin Formation in the southern Viking Graben (Folkestad and Satur, 2008). In our upper Serravallian-Tortonian sediments, the high sediment influx associated with large scale erosion of the source area during and after tectonic uplift suppresses most of the tectonic signal, and also no obvious climatic or orbital controlled cycles could be detected, similar to the ones described in the younger part of the basin fill, (Abad and Yesares Members, see e.g. Sierro et al., 2001; Krijgsman et al., 2001). Furthermore, paleoclimatic observations and modelling studies suggest warm and dry climatic conditions in SE Spain during deposition of the upper Serravalian-Tortonian succession (e.g., Zachos et al., 2001; Jiménez-Moreno, 2005; Jiménez-Moreno et al., 2010). These conditions would have a secondary effect in tectonic active settings, for instance during the progradation of coarse-grained successions into the basin.

6.1. *Normal faulting controlling high–order tectonically induced sedimentary cycles in the Sorbas basin*

Observations of normal faults offsets in the studied part of the Sorbas basin shows that the subsidence and associated accommodation space was mainly created by NE dipping normal faults, i.e. dipping towards the exposed basement and are not significantly affected by the subsequent inversion (Figs. 3 and 4). This observation means that

within this part of basin the accommodation space was created by hanging-wall tilting and filled dominantly by antithetic wedges. The sedimentation in the basin was controlled by the rate of displacement along normal faults, influencing the evolution of the slope, together with the amount and character of the sediment supply (Fig. 11).

High displacement rates along normal faults were associated with a sedimentation dominated by a discharge of coarse-grained material in shallow water environment (Fig. 11f1, i.e. facies associations A1, A2, C1 and C4, Table 1). The subsidence and slope failure by normal faulting resulted in narrowing the shelf and a retrograding depositional trend observed in proximal areas by the transition from alluvial to deltaic sediments (Fig. 7, location 1.A). The deltaic material previously trapped in shallow water environments during tectonic quiescence stages is remobilized during fault steepening and slope failure and transported deeper into the basin by toe-slope decollements and debris flows (Fig. 11a, b). Such debris flows mixing sand and clay material create the relatively isolated event beds type 1, 3 and 4 embedded within distal submarine fan deposits (Fig. 9a, c, d). Immediately after slope failure, the debris flows incorporate ambient water and material on the way leading to their partial transformation into a high-density turbiditic flow. This high-density turbiditic flow becomes stratified, due to its inability to support all particles by turbulence (e.g., Sumner et al., 2008; Postma et al., 2014). The lower layer remains concentrated and becomes supercritical. The upper layer is a low concentrated flow that transports finer fractions further into the basin plain (F8, F9, F13 and F14 facies, Table 1). The lower supercritical flow undergoes an erosive hydraulic jump and decelerate at the base of the slope (e.g., Postma et al., 2009, 2014), and is deposited as coarse-grained sediments with soft-sediment deformation, rip-ups and scours filled with upslope dipping sigmoidal crude layering (Fig. 11a, b, f; backfill, Postma et al., 2009, 2014). These scours are typical for toes of steep slopes where incoming supercritical turbulent flows suddenly decelerate and experience erosive hydraulic jump producing a cut-and-fill architecture (e.g., Mutti and Normark, 1987; Cartigny et al., 2014; Henstra et al., 2016). This process is followed by the flow becoming supercritical again, carrying coarse-grained material further into the basin and ending up as an event bed type 5 (e.g. Postma et al., 2009, 2014). Such processes create a general progradation and growth of the fan.

During the same stage of high displacement rates, sedimentation is being deposited as fining upward cycles (e.g., Fig. 7, location 1.A), as the rate of creating accommodation space is higher than the sediment supply. The exception is deposition at the toe of the slope, where the sedimentary succession is characterized by sharp contacts and a coarsening-upward trend (Fig. 11a, b, f1). Here, the base of the succession is marked by the sudden appearance of thick high-density turbidites and cohesion-less debris flows, overlaying the fine-grained sediments of the distal submarine fan and basin plain (Fig. 11b). This toe deposition is coeval with a slope steepening that may increase to 10° (Fig. 11a, b). This steepening was created mainly by normal faulting and associated antithetic rotations, combined to a lesser extent with autocyclic processes such as compensational stacking (Mutti and Sonnino, 1981; Prélat et al., 2009) or upslope knickpoint retreat (e.g. Haughton et al., 2009).

At lower displacement rates, when normal faulting gradually decreases, the creation of accommodation space is exceeded by the sediment supply (Fig. 11f2). This stage is associated with enhanced erosion in the footwall of synthetic normal faults and degradation of the source area, observed by dry mass-waste transport (i.e. rock-fall) to the immediate hanging-wall (e.g. Longhitano et al., 2015) and syn-kinematic clastic wedges filled with basement material (Fig. 10a). These sediments are subsequently remobilized and transported further into the basin by land-derived concentrated hyperpycnal flows that often bypass the delta plain and are deposited at the base of the slope or in the basin plain. This type of sedimentation is characterised by the deposition of event beds type 3 or smaller counterparts, which are often located in the apical parts of an overall coarsening-upwards trend (Figs. 9b and 11a, b). Some material was temporarily stored on the delta plain and later transported by debris flows that underwent a transformation from high- to low-density turbidity flows, sending material to the basin plain. The overall sedimentation at this stage is characterized by a progradational and aggradational depositional trend, observed as a coarsening-upward succession (Figs. 7, location 2.A and 11a, b, f2). This is recorded in proximal environments as a gradual transition from shoreface to deltaic and alluvial facies, and an increase in basement derived material (Fig. 7, location 2.A).

The periods of active normal faulting are separated by stages of tectonic quiescence, when the source area is already degraded (Fig. 11f3). This is observed by the dominantly coeval deposition of facies associations A2, B, C1, C2 and C5 (Table 1). The material shed by the source area is mainly stored temporarily in shallow water and reworked by fluvial, wave and tidal processes in a proximal shoreface environment. Intercalations of carbonate rich mudstones with abundant burrowing fauna (oysters, pectin, lithophaga) reflect a low energy environment. The main mechanisms of deposition in the deep-water environment are diluted turbiditic currents and suspension fall out, irregularly interrupted by high density flows (e.g., event bed type 6, Figs. 6n and 9f), further on transformed into diluted flows. These high density flows were most likely created by the down-dip transformation of cohesion-less to cohesive debris flows by incorporation of fine grained material (e.g., Henstra et al., 2016). This is observed by the transition from clast- to matrix-supported conglomerates in the upper part of the slope that are laterally replaced with normally graded and horizontally bedded sandstones. The decrease in the slope inclination initiated by the gradual cessation of fault activity and continued during the next tectonic quiescence stage, recongnised by a retrogradation and fining-upward trend at the toe of the slope (Fig. 11c, d, f3). In the deep water, the main mechanism of deposition is by axial flows, which rework existing sediments. This mechanism is facilitated by the reduction in coarse-grained material derived from sources perpendicular to the fault and is obvious from the direction of transport in channels in the fining upward sequence of the proximal submarine fan (Figs. 5l and 8).

In general, the higher order sedimentary cycles created by the normal faulting are characterized by successive coarsening- and fining-upward trends exceeding the inherent autocyclic character of the turbidite deposition. The instantaneous subsidence created during normal faulting resulted in slope instability, and remobilization of material from temporary storage areas located in shallow water environment and re-deposition at the base of the slope. As the erosion of coevally uplifting source area takes time to respond, more material is eroded during the subsequent stage of tectonic quiescence (e.g. Armitage et al., 2011). This is discernible in the sediments as the coarser- and thicker-parts of tectonically induced sedimentary cycles (e.g., Fig. 11b). Furthermore, the time required by the system to respond in the subsequent deposition depends also on the erodibility of the bedrock and precipitation rates. At higher erodibility and precipitation rates, the response time will be lower by enlarging the catchment area and, therefore, changing the character of deposition (e.g., Bonnet, 2009; Refice et al., 2012). This is followed by a coarsening-upward trend associated with a submarine fan growth and a net progradation into the basin that follows the deceleration of faulting activity. A fining-upward trend reflects the subsequent retrogradation due to source exhaustion during tectonic quiescence.

6.2. A low-order tectonically induced sedimentary cycle (or succession) in the Sorbas basin

The late Serravallian – Tortonian extension of the Sorbas Basin created an overall transgressive sedimentation that gradually changed from alluvial to deltaic and deeper marine. Normal fault footwall uplift and hanging-wall tilting increased the pre-existing orogenic source area that shedthe 2 km thick coarse clastic succession in the basin in 4 million years (e.g., Ott d'Estevou et al., 1990; Do Couto et al., 2014).

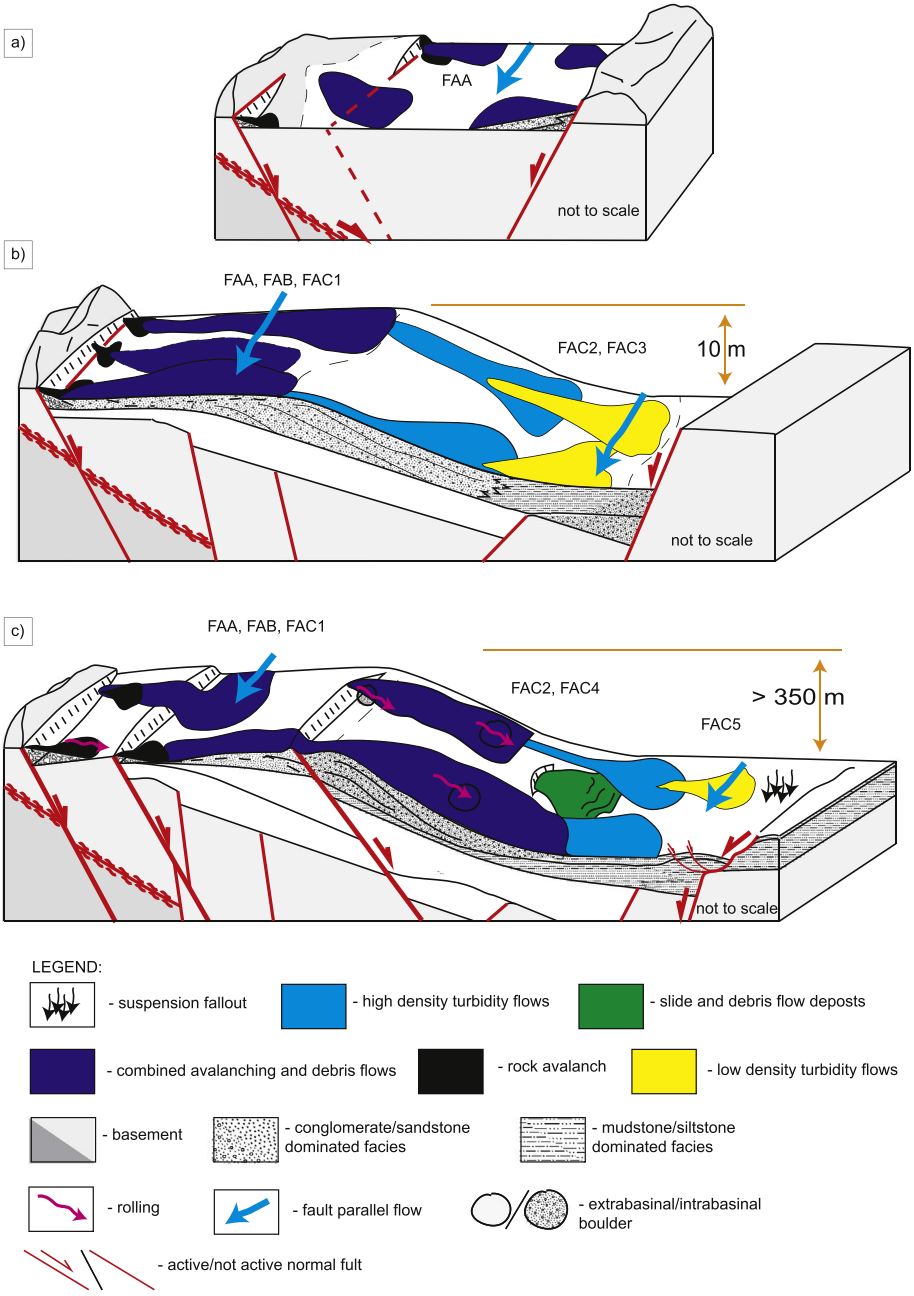

Fig. 12. Evolution of depositional environments during three stages of evolution of an asymmetric extensional basin. a) The rift initiation stage characterized by progradational and aggradational of alluvial fans sourced from immediate footwalls of normal faults creating multiple depocentres formed by the distributed deformation. No marked asymmetry is observed during this stage; b) the early rift–climax stage, when hanging–wall antithetic tilting drives the subsidence and creates an asymmetric depocentre. The depositional system is dominated by alluvial fans and shoal type fan deltas delivering material into the basin along the hanging–wall slope; c) middle–late rift climax stage dominated by coeval deposition of prograding and aggrading alluvial, delta and submarine fans, similarly controlled dominantly by the continuation of tilting through hanging-walls antithetic rotation. FAA – facies association A; FAB – facies association B; FAC1 – facies association C1; FAC2 – facies association C2; FAC3 – facies association C3; FAC4 – facies.

The initial transgression was followed by a generalized regression during the gradual cessation of normal faulting that led to the deposition of the shallow marine sediments of the Azagador Member. Our observations show that this low-order sedimentary transgressive-regressive cycle was controlled by tectonics that exceeded global sea-level oscillations, such as the drop of ~50 m between ~11 and 9 Ma, and the rise of ~35 m between ~9 and 8 Ma (Miller et al., 2005).

The high-order sedimentary cycles controlled by normal faulting described above can be grouped in three stages of coupled tectonic and sedimentological evolution in the upper Serravallian–Tortonian sedimentary succession (Fig. 12). In terms of rift sequence stratigraphy, these stages correspond to rift initiation, early rift climax and middle-late rift climax tectonic system tracts (e.g., Prosser, 1993).

Similar to what has been observed elsewhere (e.g., Leeder and Gawthorpe, 1987; Ravnas and Steel, 1998; Gawthorpe and Leeder, 2000), the first stage of rift initiation is associated with the formation of isolated fault bounded symmetric depocentres with relatively small rates of subsidence. Alluvial fan sediments were deposited in such depocentres bounded by normal faults with small displacement. The succession is characterized by a rapid transition from distal to proximal alluvial fan sediments in close proximity to the active fault (e.g., Figs. 10a and 12a). The dominant sedimentation mechanisms are rock fall and debris flows transporting footwall derived material further into the basin by a river system flowing along the axis of these depocentres. Sediments have simple wedge-shaped geometries that are directly dependent on the available accommodation space created in the normal faults hanging-walls and on the sediment supply from the immediate footwalls (e.g., Quirk, 1996).

The early rift-climax stage is represented by alluvial and delta fan deposits (Fig. 12b). Hanging-wall antithetic tilting is the main driver for basin subsidence, sedimentation and the creation of a gentle slope into the basin. The basin slope creates a shoal-type fan delta (2–5° slope dip, e.g. García-García et al., 2006), where sedimentation is dominated by gravitational flow processes such as debris and grain flows that

transform into high-density turbidity currents in deeper water (Fig. 5g). The deltaic system was deposited at the shoreface, with water depths of ~10–15 m, controlled by the subsidence created by normal faults and influenced by fluvial, wave and tidal processes.

The middle-late rift climax stage is predominately composed of delta slope and basin plain deposits (Fig. 12c). This stage occurs when the normal faulting took place dominantly inside the basin, enhancing the subsidence and creating a deeper marine environment that reached ~350 m (e.g., Ott d'Estevou et al., 1981). Normal faults offsets reach ~30 m, increasing the observed hanging-wall depositional slope to around 10°. This leads to slope failure recorded by event-beds 1, 3 and 4 (Fig. 9), the formation of a narrow shelf and dominant deposition at the toe of the slope.

The three successive stages which witnessed period of the maximum fault activity were followed by a continuation of the Tortonian sedimentation that is dominantly recorded as a cyclic alternation of packages, which contain high- and low-density turbidites that were shed from a gradually degrading source area. The low number of normal faults and the architecture of the background turbidite sedimentation indicate a predominant autocyclic nature of sedimentation, combined with episodic tectonically induced successions (see also Haughton, 2000; Haughton, 2001). The associated tectonic quiesence led to a general regression and ultimately the deposition of the shallow marine Azagador Member.

7. Conclusions

Our combined kinematic and sedimentological study of the extensive outcrop exposures in the lower part of the sedimentary infill (Upper Serravallian-Tortonian) of the Sorbas Basin showed that tectonics played dominant role during deposition. The extension changed gradually its direction from NW-SE to NE-SW during the overall transition from continental to marine sedimentation.

The mechanics of normal faulting was strongly controlled by the rheological contrast between relatively strong conglomerates and sandstones layers, and weaker siltstones and finer grained pelagic deposits. Deformation affected partially un- or poorly consolidated sediments that locally resulted in the formation of a fault gouge with a clear foliation and brittle shear bands, incorporating rheologically stronger conglomerates and sandstones blocks in wider shear zones. The rheological control is illustrated by the complex deformation along high- and low-angle normal faults, ramp-flats and staircase geometries. This complexity created a marked basin floor topography, which likely focussed turbidity currents and induced lateral migration of sedimentary lobes.

Tectonics has induced higher and lower order tectonically induced sedimentary cycles or successions. These sedimentary successions reflect series of depositional events that are not repeated regularly in the same order, unlike the climatically induced cyclicity observed in the younger part of the stratigraphic successions in the Sorbas Basin. These higher order sedimentary cycles originated as a system response to the onset of normal faulting and/or perturbation of the slip rate. Therefore, their frequency in the stratigraphic succession depends on the successive phases of activation of the normal faults. These phases are associated with the formation of syn-kinematic clastic wedges, composed of coarse-grained material supplied by fault perpendicular and fault parallel (axial) drainages formed predominantly by antithetic tilting of hanging-walls. The response time in sedimentation to alter bed thickness and create coarsening- and fining-upwards trends is controlled by the erosion of the source area and changes in the catchment geometry driven by tectonic uplift of the normal faults footwall during the asymmetric extension, likely combined with the bedrock erodibility and precipitation rates. The phases of fault activity generated the high-order sedimentary successions, which are composed of a coarsening- and fining-upward cycles. These patterns reflect the main gravity flow transformations formed in response to three main faulting stages: high displacement, gradual termination of fault activity and tectonic quiescence. The highest fault displacement rates are characterized by slope failures producing large-scale intra-basinal slumps, co-genetic debris flows and turbiditic flows that resulted in the deposition of event beds intercalated in basin plain sediments. Moreover, the slope steepening induces partial transformation of the debris flows and deposition of linked turbidites and debrites at the toe of the slope. During termination of the faulting activity, the system becomes dominated by concentrated land-derived hyperpycnal and debris flows, which did not suffer significant transformations before being deposited at the base of the slope. The tectonic quiescence stage is dominated by down-dip transformation of non-cohesive to more cohesive flows. The debris flows evolved into low-density turbiditic flows along the slope that continued further into the basin. In the sedimentary record, these flow transformations are represented as coarsening- and fining-upward cycles that reflect progradational and retrogradational depositional trends within a submarine lobe environment during the evolution of normal faulting.

The lower order tectonically induced sedimentary successions are driven by the cumulative offsets along normal faults, the migration of deformation in space and time, and the sediments distribution across multiple faults during the onset and evolution of extension. Deposition took place in alluvial, deltaic, shallow and deep marine environments during three successive phases of rift initiation and climax, followed by a general regressive stage when sedimentation was dominantly controlled by autocyclic processes. Initiation of extension was associated with the formation of isolated depocentres in continental alluvial environments, with phases of fault activation being characterized by a transition to rock-fall and proximal alluvial fans sedimentation. The continuation of extension led to the creation of a shallow-water marine environment dominated by shoal-type deltas and a deeper environment dominated by turbiditic deposition. The overall deposition was dominated by coarse-grained heterogeneous sediments originating from rock-fall, debris, turbiditic and hybrid flows, and slumps initiated on the deforming basin margin and transported along the hanging-wall slope into the deep marine environment.

Acknowledgements

This research was financed by the Netherlands Research Centre for Integrated Solid Earth Science (ISES) and the Ministry of Education, Science and Technological Development of the Republic of Serbia (project number 176019). We acknowledge helpful comments and suggestions of two anonymous reviewers that significantly improved an earlier version of the manuscript.

Appendix A. Supplementary data

Supplementary data to this article can be found online at https://doi.org/10.1016/j.gloplacha.2018.01.019.

References

Andrić, N., Sant, K., Matenco, L., Mandic, O., Tomljenović, B., Pavelić, D., Hrvatović, H., Demir, V., Ooms, J., 2017. The link between tectonics and sedimentation in asymmetric extensional basins: inferences from the study of the Sarajevo-Zenica Basin. Mar. Pet. Geol. 83, 305–332 (ISSN 0264-8172).

Armitage, J.J., Duller, R.A., Whittaker, A.C., Allen, P.A., 2011. Transformation of tectonic and climatic signals from source to sedimentary archive. Nat. Geosci. 4 (4), 231.

Arnott, R.W., Southard, J.B., 1990. Exploratory flow-duct experiments on combined-flow bed configurations, and some implications for interpreting storm-event stratification. J. Sediment. Res. 60.

Aschoff, J., Olariu, C., Steel, R., 2016. Recognition and significance of bayhead delta deposits in the rock record: a comparison of modern and ancient systems. Sedimentology 65, 62–95. http://dx.doi.org/10.1111/sed.12351.

Augier, R., Jolivet, L., Robin, C., 2005a. Late Orogenic doming in the eastern Betic Cordilleras: final exhumation of the Nevado-Filabride complex and its relation to basin genesis. Tectonics 24 (4), 1–19 (art. no. TC4003).

Augier, R., Jolivet, L., Robin, C., 2005b. Late Orogenic doming in the eastern Betic Cordilleras: final exhumation of the Nevado-Filabride complex and its relation to basin genesis. Tectonics 24.

Augier, R., Jolivet, L., Negro, F., 2013. From ductile to brittle, late-to post-orogenic evolution of the Betic Cordillera: structural insights from the northeastern Internal zones. Bull. Soc. Geol. Fr. 184, 405–425.
Balanyá, J.C., García-Dueñas, V., 1987. Les directions structurales dans le Domaine d'Alborán de part et d'autre du Détroit de Gibraltar. Comptes Rendus de l'Académie des Sciences de Paris 304 (Série II), 929e932.
Balanyá, J.C., García-Dueñas, V., Azañón, J.M., Sánchez-Gómez, M., 1997. Alternating contractional and extensional events in the Alpujarride nappes of the Alboran Domain (Betics, Gibraltar Arc). Tectonics 16, 226–238.
Balázs, A., Matenco, L., Magyar, I., Horváth, F., Cloetingh, S., 2016. The link between tectonics and sedimentation in back-arc basins: new genetic constraints from the analysis of the Pannonian Basin. Tectonics 35, 1526–1559.
Banks, C.J., Warburton, J., 1991. Mid-crustal detachment in the Betic system of southeast Spain. Tectonophysics 191, 275287–281289.
Barragán, G., 1997. Evolución geodinámica de la Depresión de Vera. Provincia de Almería. Cordilleras Béticas. Univ. Granada, Spain (PhD thesis, unpublished, 698 pp).
Barrier, L., Proust, J.-N., Nalpas, T., Robin, C., Guillocheau, F., 2010. Control of alluvial sedimentation at foreland-basin active margins: a case study from the northeastern Ebro Basin (southeastern Pyrenees, Spain). J. Sediment. Res. 80, 728–749.
Blair, T.C., McPherson, J.G., 1994. Alluvial fans and their natural distinction from rivers based on morphology, hydraulic processes, sedimentary processes, and facies assemblages. J. Sediment. Res. 64 (3), 413–467.
Blikra, L.H., Nemec, W., 1998. Postglacial colluvium in western Norway: depositional processes, facies and palaeoclimatic record. Sedimentology 45, 909–960.
Bonnet, S., 2009. Shrinking and splitting of drainage basins in orogenic landscapes from the migration of the main drainage divide. Nat. Geosci. 2, 766–771. http://dx.doi.org/10.1038/ngeo666.
Booth-Rea, G., Azaón, J.M., Goffé, B., Vidal, O., Martínez-Martínez, J.M., 2002. High-pressure, low-temperature metamorphism in Alpujarride units of southeastern Betics (Spain). Compt. Rendus Geosci. 334 (11), 857–865.
Booth-Rea, G., Azañón, J.M., Martínez-Martínez, J.M., Vidal, O., García-Dueñas, V., 2005. Contrasting structural and P-T evolution of tectonic units in the southeastern Betics: key for understanding the exhumation of the Alboran Domain HP/LT crustal rocks (western Mediterranean). Tectonics 24.
Bouma, A.H., Kuenen, P.H., Shepard, F.P., 1962. Sedimentology of some flysch deposits: a graphic approach to facies interpretation. Vol. 168 Elsevier, Amsterdam.
Braga, J.C., Martín, J.M., Betzler, C., Aguirre, J., 2006. Models of temperate carbonate deposition in Neogene basins in SE Spain: a synthesis. Geol. Soc. Lond., Spec. Publ. 255, 121–135.
Bugge, T., Belderson, R., Kenyon, N., 1988. The storegga slide. Philos. Trans. R. Soc. Lond. A Math. Phys. Eng. Sci. 325, 357–388.
Bull, S., Cartwright, J., Huuse, M., 2009. A subsurface evacuation model for submarine slope failure. Basin Res. 21, 433–443.
Carr, I.D., Gawthorpe, R.L., Jackson, C.A., Sharp, I.R., Sadek, A., 2003. Sedimentology and sequence stratigraphy of early syn-rift tidal sediments: the Nukhul Formation, Suez Rift, Egypt. J. Sediment. Res. 73, 407–420.
Cartigny, M.J., Ventra, D., Postma, G., Den Berg, J.H., 2014. Morphodynamics and sedimentary structures of bedforms under supercritical-flow conditions: new insights from flume experiments. Sedimentology 61, 712–748.
Castelltort, S., Van Den Driessche, J., 2003. How plausible are highfrequency sediment supply-driven cycles in the stratigraphic record? Sediment. Geol. 157, 3–13. http://dx.doi.org/10.1016/S0037-0738(03)00066-6.
Childs, C., Nicol, A., Walsh, J.J., Watterson, J., 1996. Growth of vertically segmented normal faults. J. Struct. Geol. 18, 1389–1397.
Childs, C., Manzocchi, T., Walsh, J.J., Bonson, C.G., Nicol, A., Schöpfer, M.P., 2009. A geometric model of fault zone and fault rock thickness variations. J. Struct. Geol. 31, 117–127.
Colella, A., 1988. Pliocene-Holocene fan deltas and braid deltas in the Crati Basin, southern Italy: a consequence of varying tectonic conditions. Fan Deltas: Sedimentology and Tectonic Settings 152, 50–74.
Comas, M., Platt, J., Soto, J., Watts, A., 1999. 44. The origin and tectonic history of the alboran basin: insights from leg 161 results. Proc. Ocean Drill. Program Sci. Results 555–580.
Crespo-Blanc, A., Orozco, M., García-Dueñas, V., 1994. Extension versus compression during the Miocene tectonic evolution of the Betic chain. Late folding of normal fault systems. Tectonics 13, 78–88.
Dabrio, C., 1990. Fan-delta facies associations in late Neogene and Quaternary basins of southeastern Spain. Coarse-Grained Deltas 91–111.
De Galdeano, C.S., Vera, J.A., 1992. Stratigraphic record and palaeogeographical context of the Neogene basins in the Betic Cordillera, Spain. Basin Res. 4, 21–35.
De Jong, K., 1991. Tectono-metamorphic Studies and Radiometric Dating in the Betic Cordilleras (SE Spain) - With Implications for the Dynamics of Extension and Compression in the Western Meditarranean area. Free University Amsterdam (PhD Thesis, 204 pp., 1991).
Dewey, J., Helman, M., Knott, S., Turco, E., Hutton, D., 1989. Kinematics of the western Mediterranean. Geol. Soc. Lond., Spec. Publ. 45, 265–283.
Do Couto, D., Gumiaux, C., Augier, R., Lebret, N., Folcher, N., Jouannic, G., Jolivet, L., Suc, J.P., Gorini, C., 2014. Tectonic inversion of an asymmetric graben: insights from a combined field and gravity survey in the Sorbas basin. Tectonics 33, 1360–1385.
Dronkert, H., 1976. Late Miocene evaporites in the Sorbas basin and adjoining areas. Mem. Soc. Geol. Ital. 16, 341–361.
Duggen, S., Hoernle, K., van den Bogaard, P., Harris, C., 2004. Magmatic evolution of the Alboran region: the role of subduction in forming the western Mediterranean and causing the Messinian Salinity Crisis. Earth Planet. Sci. Lett. 218, 91–108.
Faccenna, C., Piromallo, C., Crespo-Blanc, A., Jolivet, L., Rossetti, F., 2004. Lateral slab deformation and the origin of the western Mediterranean arcs. Tectonics 23.
Folkestad, A., Satur, N., 2008. Regressive and transgressive cycles in a rift-basin: depositional model and sedimentary partitioning of the Middle Jurassic Hugin Formation, Southern Viking Graben, North Sea. Sediment. Geol. 207 (1–4), 1–21 (ISSN 0037-0738).
Fugelli, E.M., Olsen, T.R., 2007. Delineating confined slope turbidite systems offshore mid-Norway: the Cretaceous deep-marine Lysing Formation. AAPG Bull. 91, 1577–1601.
Gabrielsen, R.H., Sokoutis, D., Willingshofer, E., Faleide, J.I., 2016. Fault linkage across weak layers during extension: an experimental approach with reference to the Hoop Fault Complex of the SW Barents Sea. Pet. Geosci. 22, 123–135.
García-Dueñas, V., Balanyá, J., Martínez-Martínez, J., 1992. Miocene extensional detachments in the outcropping basement of the northern Alboran basin (Betics) and their tectonic implications. Geo-Mar. Lett. 12, 88–95.
García-García, F., Fernández, J., Viseras, C., Soria, J.M., 2006. Architecture and sedimentary facies evolution in a delta stack controlled by fault growth (Betic Cordillera, southern Spain, late Tortonian). Sediment. Geol. 185, 79–92.
García-García, F., Corbí, H., Soria, J., Viseras, C., 2011. Architecture analysis of a river flood-dominated delta during an overall sea-level rise (early Pliocene, SE Spain). Sediment. Geol. 237, 102–113.
García-Hernández, M., López-Garrido, A., Rivas, P., Sanz de Galdeano, C., Vera, J.A., 1980. Mesozoic Palaeogeographic Evolution of the External Zones of the Betic Cordillera.
Gawthorpe, R., Leeder, M., 2000. Tectono-sedimentary evolution of active extensional basins. Basin Res. 12, 195–218.
Gawthorpe, R.L., Fraser, A.J., Collier, R.E.L., 1994. Sequence stratigraphy in active extensional basins: implications for the interpretation of ancient basin-fills. Mar. Pet. Geol. 11, 642–658.
Ge, Z., Nemec, W., Gawthorpe, R.L., Hansen, E.W.M., 2017. Response of unconfined turbidity current to normal-fault topography. Sedimentology 64, 932–959. http://dx.doi.org/10.1111/sed.12333.
Gee, M.J.R., Masson, D.G., Watts, A.B., Allen, P.A., 1999. The Saharan debris flow: an insight into the mechanics of long runout submarine debris flows. Sedimentology 46, 315–335.
Giaconia, F., Booth-Rea, G., Martínez-Martínez, J.M., Azañón, J.M., Pérez-Peña, J.V., Pérez-Romero, J., Villegas, I., 2012a. Geomorphic evidence of active tectonics in the Sierra Alhamilla (eastern Betics, SE Spain). Geomorphology 145–146, p90–106.
Giaconia, F., Booth-Rea, G., Martínez-Martínez, J.M., Azañón, J.M., Pérez-Peña, J.V., 2012b. Geomorphic analysis of the Sierra Cabrera, an active pop-up in the constrictional domain of conjugate strike-slip faults: the Palomares and Polopos fault zones (eastern Betics, SE Spain). Tectonophysics 580, 27–42.
Giaconia, F., Booth-Rea, G., Martínez-Martínez, J.M., Azañón, J.M., Pérez-Romero, J., Villegas, I., 2013. Mountain front migration and drainage captures related to fault segment linkage and growth: the Polopos transpressive fault zone (southeastern Betics, SE Spain). J. Struct. Geol. 46, 76–91.
Giaconia, F., Booth-Rea, G., Martínez-Martínez, J., Azañón, J., Storti, F., Artoni, A., 2014. Heterogeneous extension and the role of transfer faults in the development of the southeastern Betic basins (SE Spain). Tectonics 33, 2467–2489.
Gupta, S., Underhill, J., Sharp, I., Gawthorpe, R., 1999. Role of fault interactions in controlling synrift sediment dispersal patterns: Miocene, Abu Alaqa Group, Suez Rift, Sinai, Egypt. Basin Res. 11, 167–189.
Gutscher, M.A., 2012. Subduction beneath Gibraltar? Recent studies provide answers. Eos 93, 133–134.
Haughton, P.D., 1994. Deposits of deflected and ponded turbidites, currents, Sorbas Basin, southeast Spain. J. Sediment. Res. 64.
Haughton, P.D., 2000. Evolving turbidite systems on a deforming basin floor, Tabernas, SE Spain. Sedimentology 47, 497–518.
Haughton, P., 2001. Contained turbidites used to track sea bed deformation and basin migration, Sorbas Basin, south-east Spain. Basin Res. 13, 117–139.
Haughton, P.D., Barker, S.P., McCaffrey, W.D., 2003. 'Linked' debrites in sand-rich turbidite systems–origin and significance. Sedimentology 50, 459–482.
Haughton, P., Davis, C., McCaffrey, W., Barker, S., 2009. Hybrid sediment gravity flow deposits–classification, origin and significance. Mar. Pet. Geol. 26, 1900–1918.
Henstra, G.A., Grundvåg, S.-A., Johannessen, E.P., Kristensen, T.B., Midtkandal, I., Nystuen, J.P., Rotevatn, A., Surlyk, F., Sæther, T., Windelstad, J., 2016. Depositional processes and stratigraphic architecture within a coarse-grained rift-margin turbidite system: the Wollaston Forland Group, east Greenland. Mar. Pet. Geol. 76, 187–209.
Hodgson, D.M., Haughton, P.D., 2004. Impact of syndepositional faulting on gravity current behaviour and deep-water stratigraphy: Tabernas-Sorbas Basin, SE Spain. Geol. Soc. Lond., Spec. Publ. 222, 135–158.
Jabaloy, A., Galindo-Zaldívar, J., González -Lodeiro, F., 1992. The Mecina Extensional System: its relation with the post Aquitanian piggy-back basins and the paleostresses evolution (Betic Cordilleras, Spain). Geo-Mar. Lett. 12, 96–103.
Jackson, C.A.L., Kane, K.E., Larsen, E., 2010. Structural evolution of mini-basins on the Utsira High, northern North Sea: implications for Jurassic sediment dispersal and reservoir distribution. Pet. Geosci. 16, 105e120.
Jiménez-Moreno, G., 2005. Utilización del análisis polínico para la reconstrucción de la vegetación, clima y estimación de paleoaltitudes a lo largo del arco alpino europeo durante el Mioceno (21–8 Ma). Universidad de Granada, Spain (Ph.D. Dissertation, 313 pp).
Jiménez-Moreno, G., Fauquette, S., Suc, J.P., 2010. Miocene to Pliocene vegetation reconstruction and climate estimates in the Iberian Peninsula from pollen data. Rev. Palaeobot. Palynol. 162 (3), 403–415. http://dx.doi.org/10.1016/j.revpalbo.2009.08.001. (ISSN 0034-6667, 2010).
Johnson, C., 1993. Contrasted thermal histories of different nappe complexes in S.E. Spain: evidence for complex crustal extension. In: Séranne, M., Malavielle, J. (Eds.), Late Orogenic Extension in Mountain Belts. Doc. BRGM Fr., 219pp. 103.

Johnson, C., Harbury, N., Hurford, A.J., 1997. The role of extension in the Miocene denudation of the Nevado-Filábride complex, Betic Cordillera (SE Spain). Tectonics 16, 189–204.
Jolivet, L., Augier, R., Faccenna, C., Negro, F., Rimmele, G., Agard, P., Robin, C., Rossetti, F., Crespo-Blanc, A., 2008. Subduction, convergence and the mode of backarc extension in the Mediterranean region. Bull. Soc. Geol. Fr. 179, 525–550.
Jonk, R., Biermann, C., 2002. Deformation in Neogene sediments of the Sorbas and Vera Basins (SE Spain): constraints on simple-shear deformation and rigid body rotation along major strike-slip faults. J. Struct. Geol. 24, 963–977.
Kane, I.A., Pontén, A.S., 2012. Submarine transitional flow deposits in the Paleogene Gulf of Mexico. Geology 40, 1119–1122.
Kane, I.A., Pontén, A.S., Vangdal, B., Eggenhuisen, J.T., Hodgson, D.M., Spychala, Y.T., 2017. The stratigraphic record and processes of turbidity current transformation across deep-marine lobes. Sedimentology 64, 1236–1273. http://dx.doi.org/10.1111/sed.12346.
Kleverlaan, K., 1987. Gordo megabed: a possible seismite in a Tortonian submarine fan, Tabernas basin, Province Almeria, southeast Spain. Sediment. Geol. 51, 165–180.
Kleverlaan, K., 1989. Three distinctive feeder-lobe systems within one time slice of the Tortonian Tabernas fan, SE Spain. Sedimentology 36, 25–45.
Kneller, B.C., Branney, M.J., 1995. Sustained high-density turbidity currents and the deposition of thick massive sands. Sedimentology 42, 607–616.
Krijgsman, W., Fortuin, A., Hilgen, F., Sierro, F.J., 2001. Astrochronology for the Messinian Sorbas basin (SE Spain) and orbital (precessional) forcing for evaporite cyclicity. Sediment. Geol. 140, 43–60.
Leeder, M.R., Gawthorpe, R.L., 1987. Sedimentary models for extensional tilt-block/half-graben basins. Geol. Soc. Lond., Spec. Publ. 28 (1), 139–152.
Leppard, C.W., Gawthorpe, R.L., 2006. Sedimentology of rift climax deep water systems; lower rudeis formation, hammam faraun fault block, Suez Rift, Egypt. Sediment. Geol. 191, 67–87.
Lewis, M.M., Jackson, C.A.-L., Gawthorpe, R.L., Whipp, P.S., 2015. Early synrift reservoir development on the flanks of extensional forced folds: a seismic-scale outcrop analog from the Hadahid fault system, Suez rift, Egypt. AAPG Bull. 99, 985–1012.
Li, Q., Ruano, P., Pedrera, A., Galindo-Zaldívar, J., 2012. Estructura de la cuenca sedimentaria de Tabernas-Sorbas mediante prospección gravimétrica y magnética (Zonas Internas, Cordillera Bética oriental). Geogaceta 52, 117–120.
Lonergan, L., Platt, J.P., 1995. The Malaguide-Alpujarride boundary: a major extensional contact in the Internal Zone of the eastern Betic Cordillera, SE Spain. J. Struct. Geol. 17, 16551667–16651671.
Lonergan, L., White, N., 1997. Origin of the Betic–Rif mountain belt. Tectonics 16, 504–522.
Longhitano, S.G., Sabato, L., Tropeano, M., Murru, M., Carannante, G., Simone, L., Cilona, A., Vigorito, M., 2015. Outcrop reservoir analogous and porosity changes in continental deposits from an extensional basin: the case study of the upper Oligocene Sardinia Graben System, Italy. Mar. Pet. Geol. 67, 439–459.
Manzi, V., Gennari, R., Hilgen, F., Krijgsman, W., Lugli, S., Roveri, M., Sierro, F.J., 2013. Age refinement of the Messinian salinity crisis onset in the Mediterranean. Terra Nova 25 (4), 315–322.
Martín, J., Braga, J.C., 1994. Messinian events in the Sorbas Basin in southeastern Spain and their implications in the recent history of the Mediterranean. Sediment. Geol. 90, 257–268.
Martín, J.M., Braga, J.C., Sánchez-Almazo, I., 1999. The Messinian Record of the Outcropping Marginal Alboran Basin Deposits: Significance and Implications.
Martínez-Martínez, J., Azañón, J., 1997. Mode of extensional tectonics in the southeastern Betics (SE Spain): implications for the tectonic evolution of the peri-Alborán orogenic system. Tectonics 16, 205–225.
Martins-Neto, M., Catuneanu, O., 2010. Rift sequence stratigraphy. Mar. Pet. Geol. 27, 247–253.
Martín-Suárez, E., Freudenthal, M., Krijgsman, W., Fortuin, A.R., 2000. On the age of the continentaldeposits of the Zorreras Member (Sorbas Basin, SE Spain). Geobios 33, 505–512.
Meijninger, B.M.L., 2006. Late-orogenic Extension and Strike-Slip Deformation in the Neogene of Southeastern Spain. University of Utrecht (Published PhD thesis, Geologica Ultraiectina 269).
Miall, A.D., 1996. The Geology of Fluvial Deposits. Springer, New York, pp. 582.
Miller, K.G., Kominz, M.A., Browning, J.V., Wright, J.D., Mountain, G.S., Katz, M.E., Sugarman, P.J., Cramer, B.S., Christie-Blick, N., Pekar, S.F., 2005. The Phanerozoic record of global sea-level change. Science 310, 1293–1298.
Monié, P., Galindo-Zaldivar, J., Gonzalez Lodeiro, F., Goffé, B., Jabaloy, A., 1991. 40Ar/39Ar geochronology of Alpine tectonism in the Betic Cordilleras (southern Spain). J. Geol. Soc. Lond. 148, 289–297.
Montenat, C., Ott d'Estevou, P., Plaziat, J.C., Chapel, J., 1980. La signification des faunes marines contemporaines des évaporites messiniennes dans le Sud-Est de l'Espagne. Conséquences pour l'interprétation des conditions d'isolement de la Méditerranée occidentale. Géol. Mediterr. 7, 81–90.
Mulder, T., Alexander, J., 2001. Abrupt change in slope causes variation in the deposit thickness of concentrated particle-driven density currents. Mar. Geol. 175 (1), 221–235.
Mutti, E., 1992. Turbidite sandstones. Agip, Istituto di geologia, Università di Parma (275 pp).
Mutti, E., Normark, W.R., 1987. Comparing examples of modern and ancient turbidite systems: problems and concepts. In: Marine Clastic Sedimentology. Springer, pp. 1–38.
Mutti, E., Sonnino, M., 1981. Compensation cycles: a diagnostic feature of turbidite sandstone lobes. In: Int. Ass. Sed. 2nd European Meeting, Bologna, Abstracts, pp. 120–123.
Nemec, W., 1990. Aspects of sediment movement on steep delta slopes. Coarse-Grained Deltas 10, 29–73.
Nemec, W., Postma, G., 1993. Quaternary alluvial fans in southwestern Crete: sedimentation processes and geomorphic evolution. In: Alluvial Sedimentation. IAS Special Publication, vol. 17. pp. 235–276.
Nemec, W., Steel, R., 1984. Alluvial and Coastal Conglomerates: Their Significant Features and Some Comments on Gravelly Mass-flow Deposits.
Nottvedt, A., Gabrielsen, R., Steel, R., 1995. Tectonostratigraphy and sedimentary architecture of rift basins, with reference to the northern North Sea. Mar. Pet. Geol. 12, 881–901.
Ott d'Estevou, P., Termier, G., Termier, H., 1981. La spongiofaune Néogène de Sorbas (Andalousie orientale, Espagne). Géol. Mediterr. 8 (2), 61–78.
Ott d'Estevou, P., Montenat, C., Alvado, J.-C., 1990. Le bassin de Vera-Garrucha. In: Montenat, C. (Ed.), Les bassins Néogènes du domaine Bétique Oriental (Espagne). Documents et Travaux IGAL, vol. 12–13. Inst. Géol. Albert-de-Lapparent, Paris, pp. 165–187.
Pedrera, A., Galindo-Zaldívar, J., Lamas, F., Ruiz-Constán, A., 2012. Evolution of near-surface ramp-flat-ramp normal faults and implication during intramontane basin formation in the eastern Betic Cordillera (the Huércal-Overa Basin, SE Spain). Tectonics 31.
Petersen, K.D., Nielsen, S., Clausen, O., Stephenson, R., Gerya, T., 2010. Small-scale mantle convection produces stratigraphic sequences in sedimentary basins. Science 329, 827–830.
Platt, J., Vissers, R., 1989. Extensional collapse of thickened continental lithosphere: a working hypothesis for the Alboran Sea and Gibraltar arc. Geology 17, 540–543.
Platt, J., Whitehouse, M., Kelley, S., Carter, A., Hollick, L., 2003. Simultaneous extensional exhumation across the Alboran Basin: implications for the causes of late orogenic extension. Geology 31, 251–254.
Platt, J., Kelley, S., Carter, A., Orozco, M., 2005. Timing of tectonic events in the Alpujárride Complex, Betic Cordillera, southern Spain. J. Geol. Soc. 162, 451–462.
Platt, J.P., Behr, W.M., Johanesen, K., Williams, J.R., 2013. The Betic-Rif arc and its orogenic hinterland: a review. Annu. Rev. Earth Planet. Sci. 41, 313–357.
Poisson, A., Morel, J.-L., Andrieux, J., Coulon, M., Wernli, R., Guernet, C., 1999. The origin and development of Neogene basins in the SE Betic Cordillera (SE Spain): a case study of the Tabernas-Sorbas and Huercal Overa Basins. J. Pet. Geol. 22, 97–114.
Postma, G., 1984. Slumps and their deposits in fan delta front and slope. Geology 12, 27–30.
Postma, G., 1990. An analysis of the variation in delta architecture. Terra Nova 2 (2), 124–130.
Postma, G., Drinia, H., 1993. Architecture and sedimentary facies evolution of a marine, expanding outer-arc half-graben (Crete, late Miocene). Basin Res. 5, 103–124.
Postma, G., Cartigny, M., Kleverlaan, K., 2009. Structureless, coarse-tail graded Bouma Ta formed by internal hydraulic jump of the turbidity current? Sediment. Geol. 219, 1–6.
Postma, G., Kleverlaan, K., Cartigny, M.J.B., 2014. Recognition of cyclic steps in sandy and gravelly turbidite sequences, and consequences for the Bouma facies model. Sedimentology 61, 2268–2290.
Prélat, A., Hodgson, D.M., Flint, S.S., 2009. Evolution, architecture and hierarchy of distributary deep-water deposits: a high-resolution outcrop investigation from the Permian Karoo Basin, South Africa. Sedimentology 56, 2132–2154.
Prosser, S., 1993. Rift-related linked depositional systems and their seismic expression. Geol. Soc. Lond., Spec. Publ. 71, 35–66.
Puga-Bernabéu, A., Braga, J.C., Martín, J.M., 2007a. High-frequency cycles in Upper-Miocene ramp-temperate carbonates (Sorbas Basin, SE Spain). Facies 53, 329–345.
Puga-Bernabéu, Á., Martín, J.M., Braga, J.C., 2007b. Tsunami-related deposits in temperate carbonate ramps, Sorbas Basin, southern Spain. Sediment. Geol. 199 (3–4), 107–127.
Quirk, D.G., 1996. 'Base profile': a unifying concept in alluvial sequence stratigraphy. Geol. Soc. Lond., Spec. Publ. 104, 37–49.
Ravnas, R., Steel, R., 1998. Architecture of marine rift-basin successions. Am. Assoc. Pet. Geol. Bull. 82.
Refice, A., Giachetta, E., Capolongo, D., 2012. SIGNUM: a Matlab, TIN-based landscape evolution model. Comput. Geosci. 45, 293–303. http://dx.doi.org/10.1016/j.cageo.2011.11.013.
Riding, R., Martin, J.M., Braga, J.C., 1991. Coral-stromatolite reef framework, Upper Miocene, Almería, Spain. Sedimentology 38, 799–818.
Roep, T.B., Dabrio, C.J., Fortuin, A., Polo, M., 1998. Late highstand patterns of shifting and stepping coastal barriers and washover-fans (late Messinian, Sorbas Basin, SE Spain). Sediment. Geol. 116, 27–56.
Rohais, S., Eschard, R., Guillocheau, F., 2008. Depositional model and stratigraphic architecture of rift climax Gilbert-type fan deltas (Gulf of Corinth, Greece). Sediment. Geol. 210, 132–145.
Rosenbaum, G., Lister, G.S., Duboz, C., 2002. Reconstruction of the tectonic evolution of the western Mediterranean since the Oligocene. J. Virtual Explor. 8, 107–130.
Ruegg, G., 1964. Geologische Onderzoekingen in Het Bekken Van Sorbas, S Spanje. Amsterdan Geological Institute, Univ. of Amsterdan (64 pp).
Rykkelid, E., Fossen, H., 2002. Layer rotation around vertical fault overlap zones: observations from seismic data, field examples, and physical experiments. Mar. Pet. Geol. 19, 181–192.
Sanchez-Almazo, I.M., Braga, J.C., Dinares-Turell, J., MartÍN, J.M., Spiro, B., 2007. Palaeoceanographic controls on reef deposition: the Messinian Cariatiz reef (Sorbas Basin, Almería, SE Spain). Sedimentology 54, 637–660.
Schlager, W., 1993. Accommodation and supply—a dual control on stratigraphic sequences. Sediment. Geol. 86, 111–136.
Schlische, R.W., 1991. Half-graben basin filling models: new constraints on continental extensional basin development. Basin Res. 3, 123–141.
Schomacker, E.R., Kjemperud, A.V., Nystuen, J.P., Jahren, J.S., 2010. Recognition and significance of sharp-based mouth-bar deposits in the Eocene Green River Formation,

Uinta Basin, Utah. Sedimentology 57, 1069–1087.
Schöpfer, M.P., Childs, C., Walsh, J.J., 2006. Localisation of normal faults in multilayer sequences. J. Struct. Geol. 28, 816–833.
Sierro, F.J., Hilgen, F.J., Krijgsman, W., Flores, J.A., 2001. The Abad composite (SE Spain): a Messinian reference section for the Mediterranean and the APTS. Palaeogeogr. Palaeoclimatol. Palaeoecol. 168 (1–2), 141–169 (ISSN 0031-0182).
Southard, J.B., 1991. Experimental determination of bed-form stability. Annu. Rev. Earth Planet. Sci. 19, 423–455.
Spakman, W., Wortel, R., 2004. A tomographic view on western Mediterranean geodynamics. In: The TRANSMED Atlas. The Mediterranean Region From Crust to Mantle. Springer, pp. 31–52.
Spychala, Y.T., Hodgson, D.M., Stevenson, C.J., Flint, S.S., 2017. Aggradational lobe fringes: the influence of subtle intrabasinal seabed topography on sediment gravity flow processes and lobe stacking patterns. Sedimentology 64, 582–608.
Stapel, G., Moeys, R., Biermann, C., 1996. Neogene evolution of the Sorbas basin (SE Spain) determined by paleostress analysis. Tectonophysics 255, 291–305.
Stevenson, C.J., Jackson, C.A.-L., Hodgson, D.M., Hubbard, S.M., Eggenhuisen, J.T., 2015. Deep-water sediment bypass. J. Sediment. Res. 85, 1058–1081.
Strachan, L.J., Rarity, F., Gawthorpe, R.L., Wilson, P., Sharp, I., Hodgetts, D., 2013. Submarine slope processes in rift-margin basins, Miocene Suez Rift, Egypt. Geol. Soc. Am. Bull. 125, 109–127.
Stojadinović, U., Matenco, L., Andriessen, P., Toljić, M., Rundić, L., Ducea, M.N., 2017. Structure and provenance of Late Cretaceous–Miocene sediments located near the NE Dinarides margin: Inferences from kinematics of orogenic building and subsequent extensional collapse. Tectonophysics 710-711, 184 (ISSN 0040-1951).
Sumner, E., Amy, L., Talling, P., 2008. Deposit structure and processes of sand deposition from decelerating sediment suspensions. J. Sediment. Res. 78, 529–547. http://dx.doi.org/10.2110/jsr.2008.062.
Talling, P.J., Masson, D.G., Sumner, E.J., Malgesini, G., 2012. Subaqueous sediment density flows: depositional processes and deposit types. Sedimentology 59, 1937–2003.
Torres-Roldan, R.L., 1979. The tectonic subdivision of the Betic Zone (Betic Cordilleras, southern Spain); its significance and one possible geotectonic scenario for the westernmost Alpine Belt. Am. J. Sci. 279, 19–51.
Van de Poel, H.M., 1991. Messinian stratigraphy of the Nijar Basin (S.E. Spain) and the origin of its gypsum ghost limestones. Geol. Mijnb. 70, 215–234.
Vázquez, M., Jabaloy, A., Barbero, L., Stuart, F.M., 2011. Deciphering tectonic- and erosion-driven exhumation of the Nevado–Filabride Complex (Betic Cordillera, Southern Spain) by low temperature thermochronology. Terra Nova 23, 257–263.
Vissers, R.L., 2002. André Dumont medallist lecture 2011 Extension in a convergent tectonic setting: a lithospheric view on the Alboran system of SW Europe. Geol. Belg. 2012, 53–72.
Völk, H.R., 1966. Geologie et stratigraphie du Bassin Neogene de Vera. Amsterdam University, Amsterdam (Doctoral thesis, 121 pp).
Völk, H.R., Rondeel, H.E., 1964. Zur gliederung des Jungtertiärs im Becken von Vera, Südost Spanien. Geol. Mijnb. 43, 310–315.
Weijermars, R., Roep, Th.B., van den Eeckhout, B., Postma, G., Kleverlaan, K., 1985. Uplift history of a Betic fold nappe inferred from Neogene-Quaternary sedimentation and tectonics (in the Sierra Alhamilla and Almeria, Sorbas and Tabernas Basins of the Betic Cordilleras, SE Spain). Geol. Mijnb. 64, 397–411.
Whittaker, A.C., Cowie, P.A., Attal, M., Tucker, G.E., Roberts, G.P., 2007. Contrasting transient and steady-state rivers crossing active normal faults: new field observations from the Central Apennines, Italy. Basin Res. 19 (4), 529–556.
Young, M.J., Gawthorpe, R.L., Sharp, I.R., 2000. Sedimentology and sequence stratigraphy of a transfer zone coarse-grained delta, Miocene Suez Rift, Egypt. Sedimentology 47, 1081–1104.
Zachos, J.C., Pagani, M., Sloan, L., Thomas, E., Billups, K., 2001. Trends, Rhythms, and Aberrations in Global Climate 65 Ma to Present. Science 292, 686–693.